Supplementary Information

A high-resolution structural characterization and physicochemical study of how a peptoid binds to an oncoprotein MDM2

Marin Yokomine, Jumpei Morimoto,* Yasuhiro Fukuda, Takumi Ueda, Koh Takeuchi, Koji Umezawa, Hideo Ago, Hiroaki Matsuura, Go Ueno, Akinobu Senoo, Satoru Nagatoishi, Kouhei Tsumoto and Shinsuke Sando*

Table of Contents

Materials and Methods

Abbreviations for chemical compounds.

DMF, *N*,*N*-dimethylformamide; DCM, dichloromethane; DIPEA, *N*,*N*-diisopropylethylamine; DMSO, dimethyl sulfoxide; THF, tetrahydrofuran; MeOH, methanol; ACN, acetonitrile; TEAA, triethylammonium acetate solution; TEA, triethylamine; BME, 2-mercaptoethanol; NHS, *N*-hydroxysuccinimide; EDC·HCl, 1-(3-dimethylaminopropyl)-3-ethylcarbodiimide hydrochloride.

General remarks.

All quantum chemical calculations were carried out with the Gaussian16 package[1]. Molecular graphics and analyses were performed with UCSF ChimeraX[2–4] or UCSF Chimera[5]. Distilled water was further purified with Millipore Milli-Q (Milli-Q Reference, Merck).

General remarks for synthesis.

Chemicals and solvents used in this study were purchased from commercial suppliers and used without further purification. Preparative high performance liquid chromatography (HPLC) was performed on a Prominence HPLC system (Shimadzu) with a 5C18-AR-II column (Nacalai tesque, 10 mm I.D.×150 mm, 34350-41). Ultra-performance liquid chromatography (UPLC) and liquid chromatography-mass spectrometry (LC-MS) were performed on an ACQUITY UPLC H-Class/SQD2 (Waters) using ACQUITY UPLC BEH C18 column (Waters, 2.1 mm I.D. × 50 mm). HRMS data was obtained using ACQUITYUPLC H-Class/Xevo G3 QTof (Waters) with a ACQUITY^{TM} Premier Peptide BEH C_{18} Column (Waters, 2.1 mm I.D. × 100 mm).

General procedures for the synthesis of peptoids with piperazinyl C-termini (2–5).

Objective compounds were synthesized on resin, cleaved, and purified as previously described.[6–8]

General procedures for synthesis of peptoids with ethylenediamine C-termini (2–5-Sar$_3$-EDA, S1–S4-Sar$_3$-EDA).

Trityl resin was swelled with a minimal volume of anhydrous THF in a syringe for 10 min. Ethylenediamine (20 equiv., 1 M) in anhydrous THF was added to the resin. After shaking for 2 h, the resin was washed with THF and DCM three times each. The resin was treated with 85/10/5 DCM/MeOH/DIPEA solution for 15 min and washed with DCM and DMF three times each. After loading ethylenediamine, oligomers were synthesized on resin, cleaved, and purified as previously described.[6–8]

General procedures for the synthesis of peptoids with fluorescein-labeled ethylenediamine C-termini (2–5-Sar$_3$-EDA-Flu, S1–S4-Sar$_3$-EDA-Flu).

DMSO solution of a peptoid with ethylenediamine C-terminus (0.50 μmol) was added to an Eppendorf tube. 5/6-Carboxyfluorescein *N*-succinimidyl ester (1.0 μmol, 2.0 equiv.) and TEA (1.0 μmol, 2.0 equiv.) dissolved in 25 μL DMF was added, and the reaction mixture was shaken at room temperature overnight. 6.25 μL of piperidine was added, and the reaction mixture was shaken at room temperature for 60–100 min. These reactions were conducted in the dark. The solution was diluted with ACN and water, and purified by a reversed

phase column on HPLC using ACN and 100 mM TEAA (pH 7.0) as solvents. Of the compounds with the objective molecular weight but different HPLC retention times, the one that eluted first was lyophilized and dissolved in DMSO. The obtained compound was quantified from UV absorbance derived from carboxyfluorescein (ε_{495} = 75,000 M^{-1} cm^{-1}).

Synthesis of oligo-NSA 2.

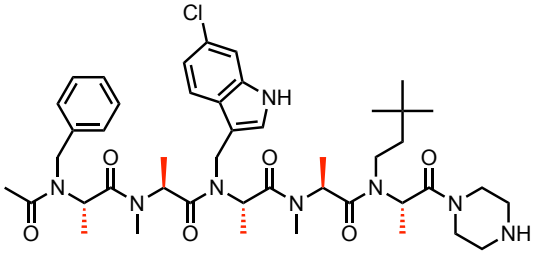

23.3 mg of trityl chloride resin (1.78 mmol/g, 41.5 μmol) was used for synthesis. Fmoc-Ala-OH, Fmoc-*N*-Me-Ala-OH, 3,3-dimethylbutyraldehyde, 6-chloroindole-3-carboxaldehyde and benzaldehyde were used as building blocks. Yield: 11%. HRMS (ESI-TOF MS) *m/z*: $[M + H]^+$ Calcd for $C_{45}H_{66}ClN_8O_6^+$ 849.4788; Found 849.4814.

Synthesis of oligo-NSA 2-Sar$_3$-EDA.

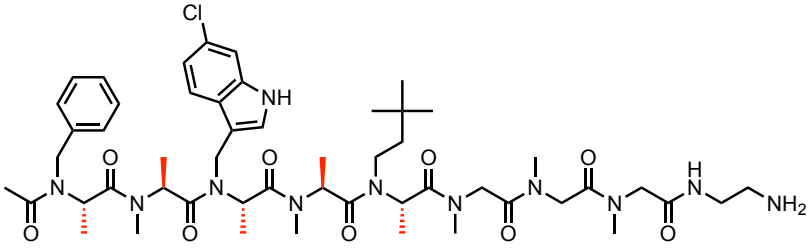

22.5 mg of trityl chloride resin (1.78 mmol/g, 40.0 μmol) was used for synthesis. Fmoc-Sar-OH, Fmoc-Ala-OH, Fmoc-*N*-Me-Ala-OH, 3,3-dimethylbutyraldehyde, 6-chloroindole-3-carboxaldehyde and benzaldehyde were used as building blocks. Yield: 23%. HRMS (ESI-TOF MS) *m/z*: $[M + H]^+$ Calcd for $C_{52}H_{79}ClN_{11}O_9^+$ 1036.5745; Found 1036.5773.

Synthesis of oligo-NSA 2-Sar$_3$-EDA-Flu.

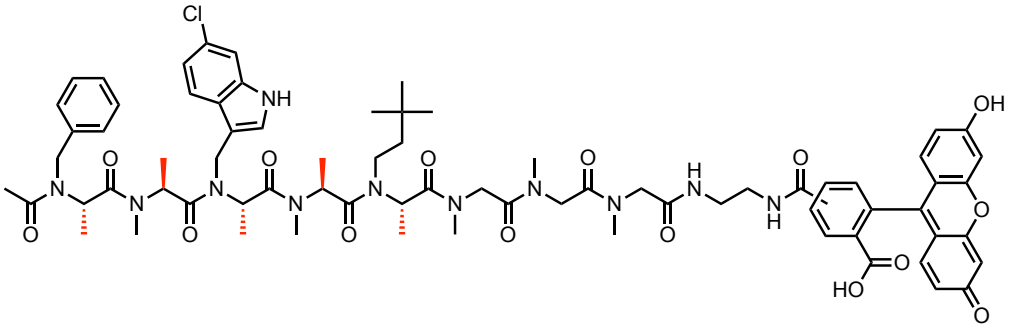

8.03 μL of 62.3 mM **oligo-NSA 2-Sar$_3$-EDA** in DMSO was used. Yield: 14%. HRMS (ESI-TOF MS) *m/z*: $[M + H]^+$ Calcd for $C_{73}H_{89}ClN_{11}O_{15}^+$ 1394.6223; Found 1394.6223.

Synthesis of oligo-NSA/G 3.

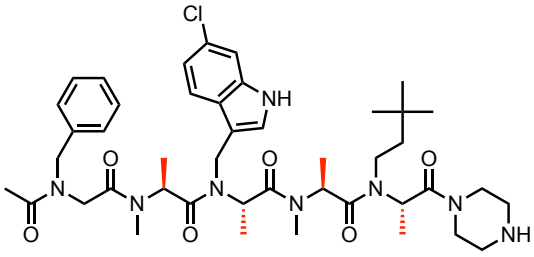

10.3 mg of trityl chloride resin (1.78 mmol/g, 18.3 μmol) was used for synthesis. Fmoc-Ala-OH, Fmoc-*N*-Me-Ala-OH, Fmoc-Gly-OH, 3,3-dimethylbutyraldehyde, 6-cloroindole-3-carboxaldehyde and benzaldehyde were used as building blocks. Yield: 39%. HRMS (ESI-TOF MS) *m/z*: $[M + H]^+$ Calcd for $C_{44}H_{64}ClN_8O_6^+$ 835.4632; Found 835.4660.

Synthesis of oligo-NSA/G 3-Sar$_3$-EDA.

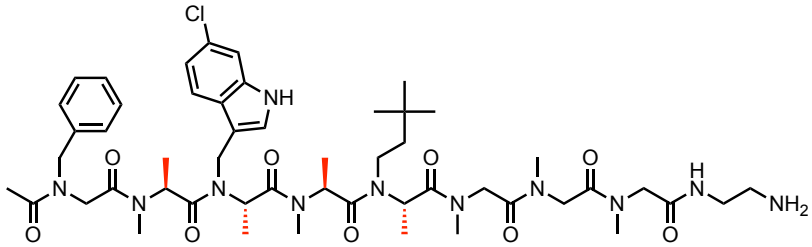

26.2 mg of trityl chloride resin (1.55 mmol/g, 40.5 μmol) was used for synthesis. Fmoc-Sar-OH, Fmoc-Ala-OH, Fmoc-*N*-Me-Ala-OH, Fmoc-Gly-OH, 3,3-dimethylbutyraldehyde, 6-chloroindole-3-carboxaldehyde and benzaldehyde were used as building blocks. Yield: 24%. HRMS (ESI-TOF MS) *m/z*: $[M + H]^+$ Calcd for $C_{51}H_{77}ClN_{11}O_9^+$ 1022.5589; Found 1022.5624.

Synthesis of oligo-NSA/G 3-Sar$_3$-EDA-Flu.

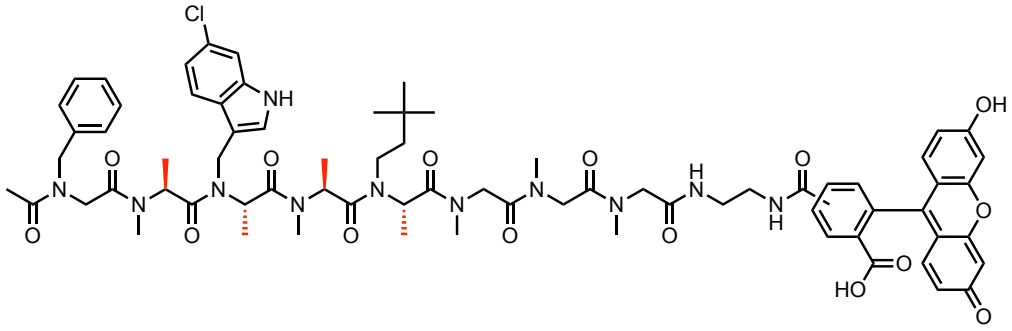

3.91 μL of 128 mM **oligo-NSA/G 3-Sar$_3$-EDA** in DMSO was used. Yield: 16%. HRMS (ESI-TOF MS) *m/z*: $[M + H]^+$ Calcd for $C_{72}H_{87}ClN_{11}O_{15}^+$ 1380.6066; Found 1380.6052.

Synthesis of oligo-NSA/G 4.

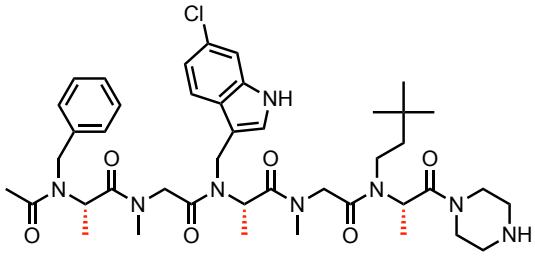

23.9 mg of trityl chloride resin (1.78 mmol/g, 42.5 μmol) was used for synthesis. Fmoc-Ala-OH, Fmoc-Sar-OH, 3,3-dimethylbutyraldehyde, 6-chloroindole-3-carboxaldehyde and benzaldehyde were used as building blocks. Yield: 28%. HRMS (ESI-TOF MS) *m/z*: $[M + H]^+$ Calcd for $C_{43}H_{62}ClN_8O_6^+$ 821.4475; Found 821.4481.

Synthesis of oligo-NSA/G 4-Sar$_3$-EDA.

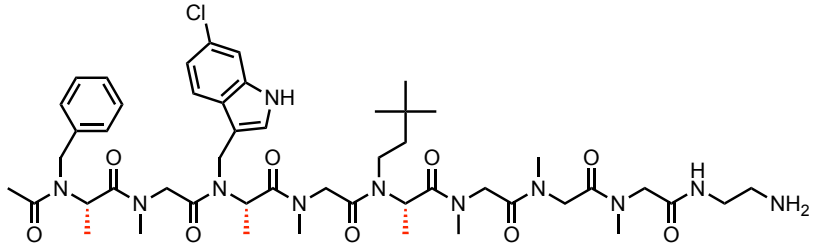

22.5 mg of trityl chloride resin (1.78 mmol/g, 40.0 μmol) was used for synthesis. Fmoc-Sar-OH, Fmoc-Ala-OH, 3,3-dimethylbutyraldehyde, 6-chloroindole-3-carboxaldehyde and benzaldehyde were used as building blocks. Yield: 31%. HRMS (ESI-TOF MS) *m/z*: $[M + H]^+$ Calcd for $C_{50}H_{75}ClN_{11}O_9^+$ 1008.5432; Found 1008.5444.

Synthesis of oligo-NSA/G 4-Sar$_3$-EDA-Flu.

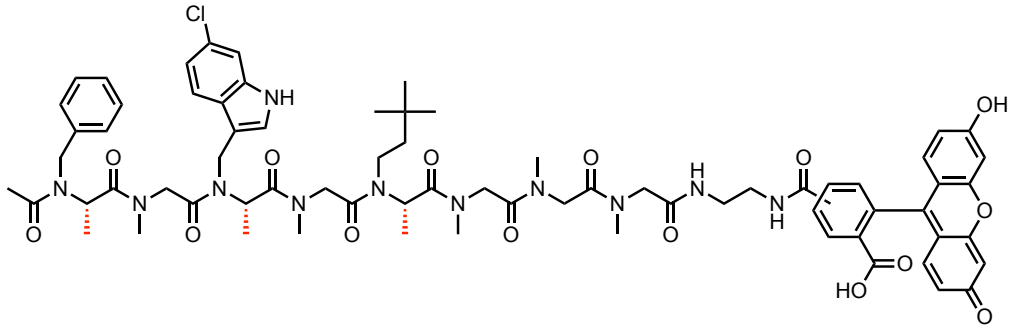

5.98 μL of 83.7 mM **oligo-NSA/G 4-Sar$_3$-EDA** in DMSO was used. Yield: 15%. HRMS (ESI-TOF MS) *m/z*: $[M + H]^+$ Calcd for $C_{71}H_{85}ClN_{11}O_{15}^+$ 1366.5910; Found 1366.5948.

Synthesis of oligo-NSG 5.

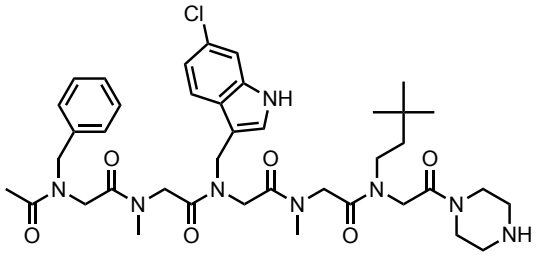

23.2 mg of trityl chloride resin (1.78 mmol/g, 41.3 μmol) was used for synthesis. Fmoc-Gly-OH, Fmoc-Sar-OH, 3,3-dimethylbutyraldehyde, 6-chloroindole-3-carboxaldehyde and benzaldehyde were used as building blocks. Yield: 20%. HRMS (ESI-TOF MS) *m/z*: $[M + H]^+$ Calcd for $C_{40}H_{56}ClN_8O_6^+$ 779.4006; Found 779.4006.

Synthesis of oligo-NSG 5-Sar$_3$-EDA.

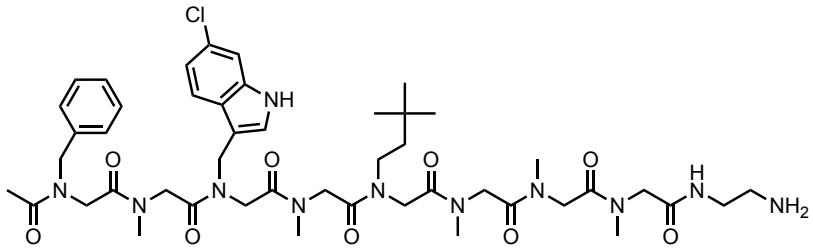

22.5 mg of trityl chloride resin (1.78 mmol/g, 40.0 μmol) was used for synthesis. Fmoc-Sar-OH, Fmoc-Gly-OH, 3,3-dimethylbutyraldehyde, 6-chloroindole-3-carboxaldehyde and benzaldehyde were used as building blocks. Yield: 25%. HRMS (ESI-TOF MS) *m/z*: $[M + H]^+$ Calcd for $C_{47}H_{69}ClN_{11}O_9^+$ 966.4963; Found 966.4934.

Synthesis of oligo-NSG 5-Sar$_3$-EDA-Flu.

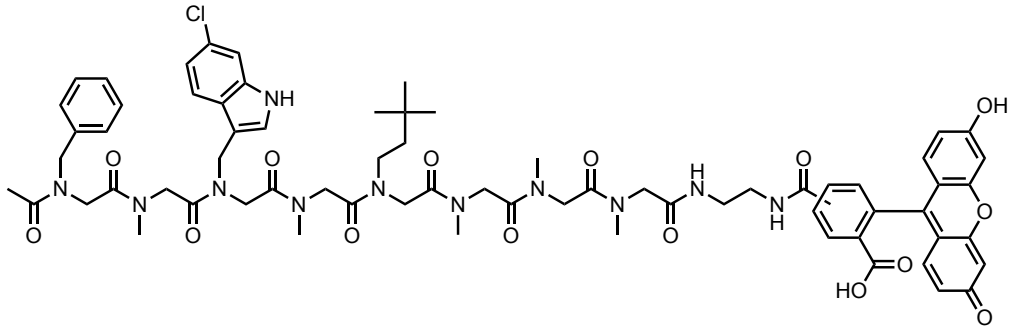

6.83 μL of 73.2 mM **oligo-NSG 5-Sar$_3$-EDA** in DMSO was used. Yield: 14%. HRMS (ESI-TOF MS) *m/z*: $[M + H]^+$ Calcd for $C_{68}H_{79}ClN_{11}O_{15}^+$ 1324.5440; Found 1324.5468.

Synthesis of oligo-NSA/G S1-Sar$_3$-EDA.

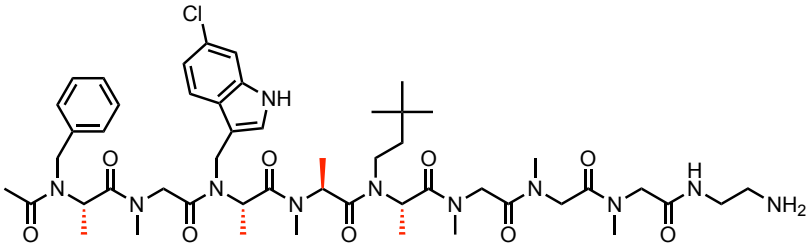

26.2 mg of trityl chloride resin (1.55 mmol/g, 40.5 μmol) was used for synthesis. Fmoc-Sar-OH, Fmoc-Ala-OH, Fmoc-*N*-Me-Ala-OH, 3,3-dimethylbutyraldehyde, 6-chloroindole-3-carboxaldehyde and benzaldehyde were used as building blocks. Yield: 25%. HRMS (ESI-TOF MS) *m/z*: $[M + H]^+$ Calcd for $C_{51}H_{77}ClN_{11}O_9^+$ 1022.5589; Found 1022.5599.

Synthesis of oligo-NSA/G S1-Sar$_3$-EDA-Flu.

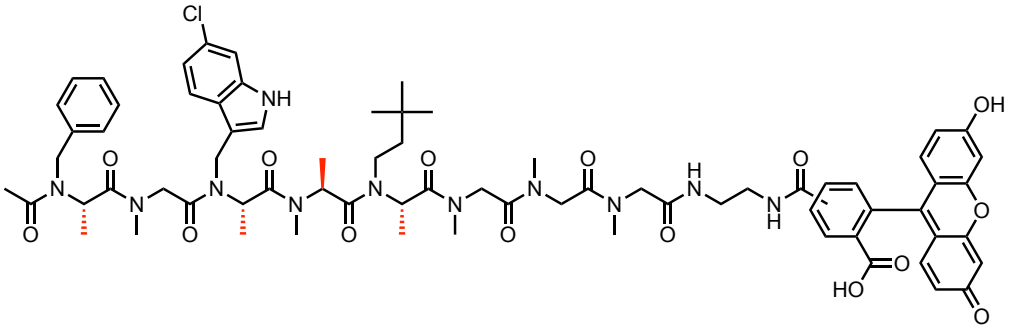

3.69 μL of 135 mM **oligo-NSA/G S1-Sar$_3$-EDA** in DMSO was used. Yield: 13%. HRMS (ESI-TOF MS) *m/z*: $[M + H]^+$ Calcd for $C_{72}H_{87}ClN_{11}O_{15}^+$ 1380.6066; Found 1380.6041.

Synthesis of oligo-NSA/G S2-Sar$_3$-EDA.

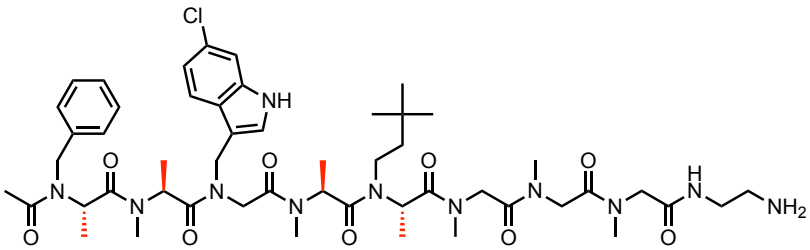

26.2 mg of trityl chloride resin (1.55 mmol/g, 40.5 μmol) was used for synthesis. Fmoc-Sar-OH, Fmoc-Ala-OH, Fmoc-*N*-Me-Ala-OH, Fmoc-Gly-OH, 3,3-dimethylbutyraldehyde, 6-chloroindole-3-carboxaldehyde and benzaldehyde were used as building blocks. Yield: 22%. HRMS (ESI-TOF MS) *m/z*: $[M + H]^+$ Calcd for $C_{51}H_{77}ClN_{11}O_9^+$ 1022.5589; Found 1022.5583.

Synthesis of oligo-NSA/G S2-Sar$_3$-EDA-Flu.

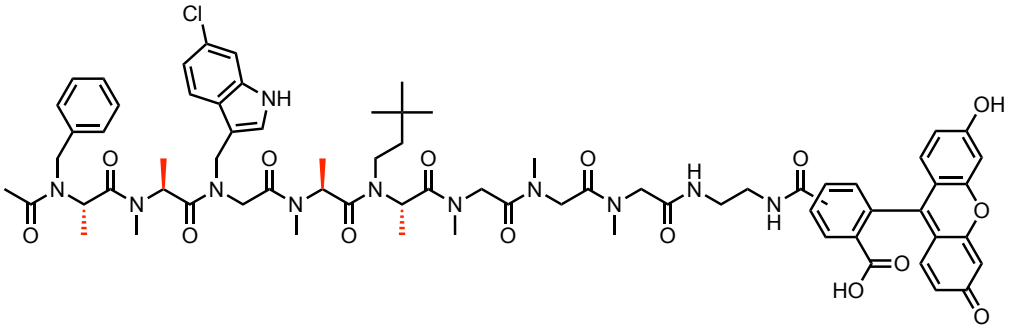

4.24 μL of 118 mM **oligo-NSA/G S2-Sar$_3$-EDA** in DMSO was used. Yield: 13%. HRMS (ESI-TOF MS) *m/z*: $[M + H]^+$ Calcd for $C_{72}H_{87}ClN_{11}O_{15}^+$ 1380.6066; Found 1380.6061.

Synthesis of oligo-NSA/G S3-Sar$_3$-EDA.

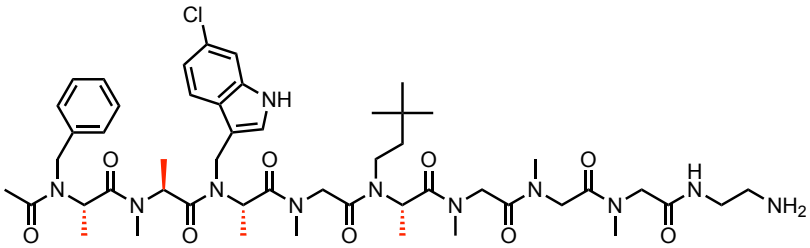

26.2 mg of trityl chloride resin (1.55 mmol/g, 40.5 μmol) was used for synthesis. Fmoc-Sar-OH, Fmoc-Ala-OH, Fmoc-*N*-Me-Ala-OH, 3,3-dimethylbutyraldehyde, 6-chloroindole-3-carboxaldehyde and benzaldehyde were used as building blocks. Yield: 29%. HRMS (ESI-TOF MS) *m/z*: $[M + H]^+$ Calcd for $C_{51}H_{77}ClN_{11}O_9^+$ 1022.5589; Found 1022.5605.

Synthesis of oligo-NSA/G S3-Sar$_3$-EDA-Flu.

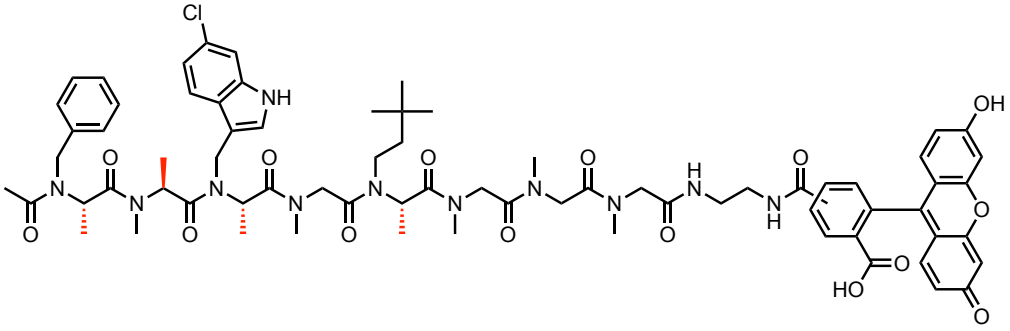

3.21 μL of 156 mM **oligo-NSA/G S3-Sar$_3$-EDA** in DMSO was used. Yield: 16%. HRMS (ESI-TOF MS) *m/z*: $[M + H]^+$ Calcd for $C_{72}H_{87}ClN_{11}O_{15}^+$ 1380.6066; Found 1380.6130.

Synthesis of oligo-NSA/G S4-Sar$_3$-EDA.

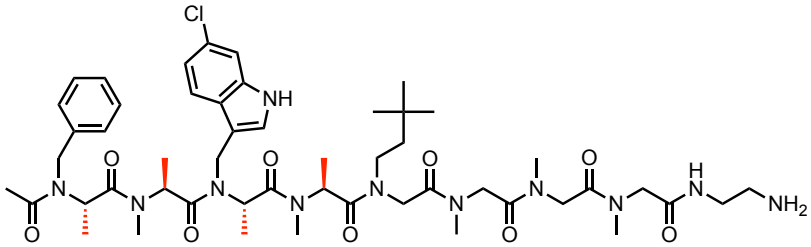

26.2 mg of trityl chloride resin (1.55 mmol/g, 40.5 μmol) was used for synthesis. Fmoc-Sar-OH, Fmoc-Gly-OH, Fmoc-*N*-Me-Ala-OH, Fmoc-Ala-OH, 3,3-dimethylbutyraldehyde, 6-chloroindole-3-carboxaldehyde and benzaldehyde were used as building blocks. Yield: 13%. HRMS (ESI-TOF MS) *m/z*: $[M + H]^+$ Calcd for $C_{51}H_{77}ClN_{11}O_9^+$ 1022.5589; Found 1022.5570.

Synthesis of oligo-NSA/G S4-Sar$_3$-EDA-Flu.

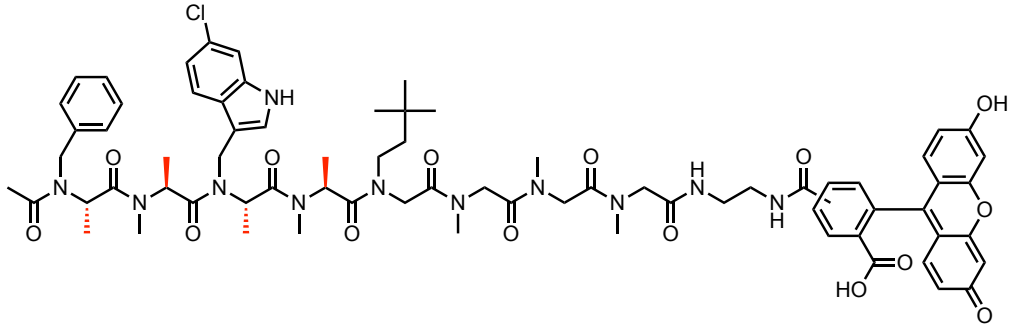

7.11 μL of 70.3 mM **oligo-NSA/G S4-Sar$_3$-EDA** in DMSO was used. Only one peak of the compound of the target molecular weight was seen. Yield: 33%. HRMS (ESI-TOF MS) *m/z*: $[M + H]^+$ Calcd for $C_{72}H_{87}ClN_{11}O_{15}^+$ 1380.6066; Found 1380.6062.

Recombinant expression and purification of MDM2 (17–111) and co-crystallization with NSA-type peptoid 2.

Human MDM2 (17–111) used for crystal structural analysis was expressed using pGEX-6P-2 vectors in BL21(DE3)pLysS cells grown in LB medium. Expression of MDM2 was induced by adding IPTG to the final concentration of 1 mM when the OD_{600} reached to 0.6. The induction was performed at 18 °C for 4 h with continuous shaking and cultures were centrifuged at 7,000 g for 10 min at 4 °C. Subsequent purification was performed as for MDM2 (17–125). After size exclusion chromatography, fractions containing MDM2 were combined and the buffer was exchanged to 5 mM Tris-HCl (pH = 8.0), 50 mM NaCl, 5 mM BME. MDM2 was concentrated to 11.7 mg mL^{-1} using Amicon Ultra 3K.

The complex was then formed by combining MDM2 with ca. twice molar excess of **2** in DMSO and this solution containing 5% DMSO was allowed to sit overnight at 4 °C, and centrifuged at 10,000 g for 10 min at 4 °C. MDM2 and **2** were co-crystallized via sitting vapor-diffusion method by mixing 0.5 μL MDM2/**2** with 0.5 μL reservoir solution consisting of 1 M sodium acetate trihydrate (pH = 4.5), 3 M NaCl at 20 °C. The needle-shaped crystals grew. Each crystal was briefly soaked in a cryoprotectant solution consisting of the reservoir solution supplemented with 20% (v/v) glycerol dissolved in their corresponding mother liquors, and then flash-cooled directly using a liquid-nitrogen.

Data collection and structure determination.

Data collection for MDM2/**2** complex co-crystal was performed with *ZOO*[9], an automated data collection system installed at BL32XU beamline in SPring-8. The data set were obtained using a continuous helical scheme with the following experimental parameters: wavelength, 1Å; total oscillation, 360°; oscillation width per frame, 0.1°; exposure time, 0.02 s; temperature, 100 K; beam size, 10 μm (H) × 15 μm (V); average dose per crystal volume, 10 MGy; detector EIGER X 9M (Dectris Ltd.). The collected data set was processed by *XDS/XSCALE*[10] using an automated data processing pipeline *KAMO*[11].

The initial model of MDM2 was determined by the molecular replacement method with the MDM2 search model which was extracted from the MDM2 and peptide complex crystal structure (PDB ID: 5AFG)[12]. The model of **2** was included manually based on the 2m|*F*o| - D|*F*c| and m|*F*o| - D|*F*c| residual electron density maps in the following iterative structure refinement cycles. The crystallographic R and R_{free} of MDM2/**2** complex model were converged to 0.169 and 0.190, respectively. There were no Ramachandran outliers in the refined model. The maximum resolution of diffraction data used for the structure refinement, which was determined based on the statistics from the structure refinement, was 1.35 Å resolution. The computer programs for molecular replacement method, structure refinement, manual model building, and preparation of structural dictionary of the **2** for the structure refinement and manual model building were phenix.phaser, phenix.refine, coot in CCP4, and phenix.elbow, respectively[13,14].

Recombinant expression and purification of MDM2 (17–125).

Human MDM2 (17–125) used for binding assays was expressed using pGEX-6P-2 vectors in BL21(DE3)pLysS cells grown in LB medium as previously described.[6,7] The pGEX-6P-2-MDM2 (17–125) was a gift from Gary Daughdrill (Addgene plasmid # 62063).[15]

FA binding assay of peptoids with fluorescent-labeled ethylenediamine C-termini (Table S2 and Fig. S26).

FA binding assays of peptoids with fluorescein-labeled ethylenediamine C-termini (**2**–**5-Sar$_3$-EDA-Flu**, **S1**–**S4-Sar$_3$-EDA-Flu**) with MDM2 (17–125) were conducted as previously described.[7] Peptoids with fluorescein-labeled ethylenediamine C-termini were used at 10 nM. FA was measured on a plate reader (SpectraMax® Paradigm® Multi-Mode Detection Platform, Molecular Devices) at 25 °C. Excitation wavelength and emission wavelength were set to 485 nm and 535 nm, respectively. Dissociation constant (K_D) values were calculated using parameters determined by fitting the plot to the following equation: $y = y_{min} + (y_{max} - y_{min})/(1 + (K_D/x)^n)$. x, y, and n denote MDM2 concentration, ΔFA, and hill coefficient, respectively.

NMR spectroscopic studies of peptoids.

NMR spectra of **2**–**5** were recorded at 1–10 mM in 20–100% DMSO-d_6/D_2O on a Bruker Avance III HD 800 or Avance III 500 spectrometer equipped with a cryogenic probe. HMBC spectrum was recorded with x points of 2,048 (complex), y points of 2,048, relaxation delay of 1 s, and receiver gain of 203. HSQC spectrum was recorded with x points of 1,024, y points of 512, relaxation delay of 1 s and receiver gain of 203. ROESY spectrum was recorded with relaxation delay of 1 s, mixing time of 250 ms, and receiver gain of 203. TOCSY

spectrum was recorded with x points of 1,024 or 2,048, y points of 512 or 1,024, relaxation delay of 1 s, mixing time of 60 ms, and receiver gain of 203. Chemical shifts of ^{1}H NMR, HMBC, HSQC, ROESY, and TOCSY spectra are reported in p.p.m relative to 4,4-dimethyl-4-silapentane-1-sulfonic acid as external standards. Assignment of ^{1}H NMR was assisted by HMBC and HSQC spectrum as previously described.[6,8]

Cis-trans isomerization state of each peptide bond in **3** was identified using a sample dissolved in DMSO-d_6 (Fig. S6–S9). The *cis-trans* isomerization state in 20% DMSO-d_6/D_2O = 20:80 was determined using continuous chemical shift change upon adding D_2O to **3** in DMSO-d_6 (Fig. S10).

MD simulations of free peptoids.

MD simulations of **2**–**5** were conducted using Amber 2022[16]. Partial charges of peptoids were fitted to the electrostatic potential calculated by density functional theory (B3LYP/6-31G(d,p)) calculation using the restrained electrostatic potential (RESP) method through the antechamber module of AmberTools22. The other parameters were obtained using the general AMBER force field 2 (GAFF2). The initial structures were constructed from the crystal structure of **2** with MDM2 with modifications to specific atoms as required. The system was charge neutralized by Cl^- ions and solvated with TIP3P water in truncated octahedral boxes with a 15 Å buffer using the LEaP module of AmberTools22[16]. The periodic boundary conditions were applied, and the long-range electrostatic interactions were calculated with Particle-Mesh Ewald method[17]. The system was energy-minimized for 500 steps with the steepest descent algorithm and then 500 steps with the conjugate gradient algorithm with a 10 Å nonbonded cutoff, and then energy-minimized again for 1,000 steps with the steepest descent algorithm and then 1,500 steps with the conjugate gradient algorithm with a 10 Å non-bonded cutoff. MD simulation was performed consisting of 1 ns gradual heating (from 1 K to 298 K) under NVT system, 1 ns equilibration under NVT system, 1 ns equilibration under NPT system, and 500 ns production procedures under NPT system at 298 K. MD simulations after the energy minimization were performed 5 times each. The cpptraj module of AmberTools22 was used to analyze the trajectories generated from MD simulations.

ITC measurement of peptoids and MDM2 (Fig. S27).

ITC measurements of **2**–**5** were conducted in PBS at 25 °C on an MicroCal PEAQ-ITC (Malvern Panalytical) as previously described. 100 μM (**2**), 200 μM (**3**), or 500 μM (**4**, **5**) solution of peptoid in PBS was titrated into a solution of MDM2 (17–125) in PBS, with concentrations of 10 μM for **2**, 20 μM for **3**, or 50 μM for **4** and **5**. The recorded heat was plotted against the molar ratio of MDM2 and the plot was fitted to generate a binding curve by applying a one-site model using MicroCal PEAQ-ITC Analysis Software. ΔH and K_D values were determined from the fitting of the plot and then ΔG and ΔS were determined using the following two equations: (1) $\Delta G = RT\ln\Delta K_D$ and (2) $\Delta S = (\Delta H - \Delta G)/T$.

SPR measurement of peptoids with ethylenediamine C-termini (Fig. S28, S29).

SPR measurements (single cycle kinetics) of peptoids with ethylenediamine C-termini (**2–4-Sar$_3$-EDA**) with MDM2 (17–125) were performed on Biacore T100 (GE Healthcare) using the Series S Sensor Chip CM5 (Cytiva). Peptoids-EDA were immobilized on the sensor chip using amine coupling chemistry (7 min 0.05 M NHS/0.2 M EDC·HCl, 12 s 100 μM (**2-Sar$_3$-EDA**) or 70 μM (**3**, **4-Sar$_3$-EDA**) peptoid in 10 mM Borate/1 M

NaCl buffer (pH = 8.5), and 7 min 1 M ethanolamine). The immobilized amounts of **2-Sar$_3$-EDA**, **3-Sar$_3$-EDA**, and **4-Sar$_3$-EDA** were 37, 23, and 22 RUs, respectively. MDM2 (0.94–15 nM for **2-Sar$_3$-EDA**, 12–1000 nM for **3-Sar$_3$-EDA**, and 74–6000 nM for **4-Sar$_3$-EDA**) was injected onto the peptoid-immobilized sensor chip at a flow rate of 30 μL/min (10 °C, running buffer: PBS (pH 7.4) containing 0.01% Tween 20, contact time: 3 min, final dissociation time: 3 min). The sensorgrams were fitted to a 1:1 binding model for kinetic analysis. The plots were fitted to a steady-state affinity model for affinity analysis.

MD simulations of free MDM2.

MD simulations of MDM2 were conducted using Amber 2022[16]. The initial structure was constructed by complementing some of the missing residues (17–24) of MDM2 in the crystal structure of **2** and MDM2 using Modeller[18] and capping the N-terminus with an acetyl group and the C-terminus with an *N*-methyl group. The system was charge neutralized by Cl^- ions and solvated with TIP3P water in truncated octahedral boxes with a 15 Å buffer using the LEaP module of AmberTools22[16] using ff14SB force field. The periodic boundary conditions were applied, and the long-range electrostatic interactions were calculated with Particle-Mesh Ewald method[17]. The system was energy-minimized for 500 steps with the steepest descent algorithm and then 500 steps with the conjugate gradient algorithm with a 10 Å nonbonded cutoff with positional restraints of 100 kcal/(mol Å^2) on the backbone atoms of MDM2. Then, 1 ns gradual heating (from 1 K to 298 K) under NVT system, 1 ns equilibration under NVT system, 2 ns equilibration under NPT system with positional restraints of 100 kcal/(mol Å^2) on the backbone atoms of MDM2 were performed. Subsequently, 2 ns equilibration with weaker positional restraints (10 kcal/(mol Å^2)) and without restraints under NPT system, and 200 ns production procedures under NPT system at 298 K were performed. MD simulations after the energy minimization were performed 5 times. The cpptraj module of AmberTools22 was used to analyze the trajectories generated from MD simulations.

MD simulations of the complex of peptoids with MDM2.

MD simulations of **2**, **4**, or **5** with MDM2 were conducted using Amber 2022[16]. The initial structures, peptoids force fields, and MDM2 force fields were prepared using the same method as for the MD simulations of free peptoids or free MDM2. Solvation, energy-minimization, equilibration, and production were performed using the same method as for the MD simulations of free MDM2 with restraints on the non-hydrogen atoms of the peptoids and the backbone of MDM2.

Supporting Figures & Tables

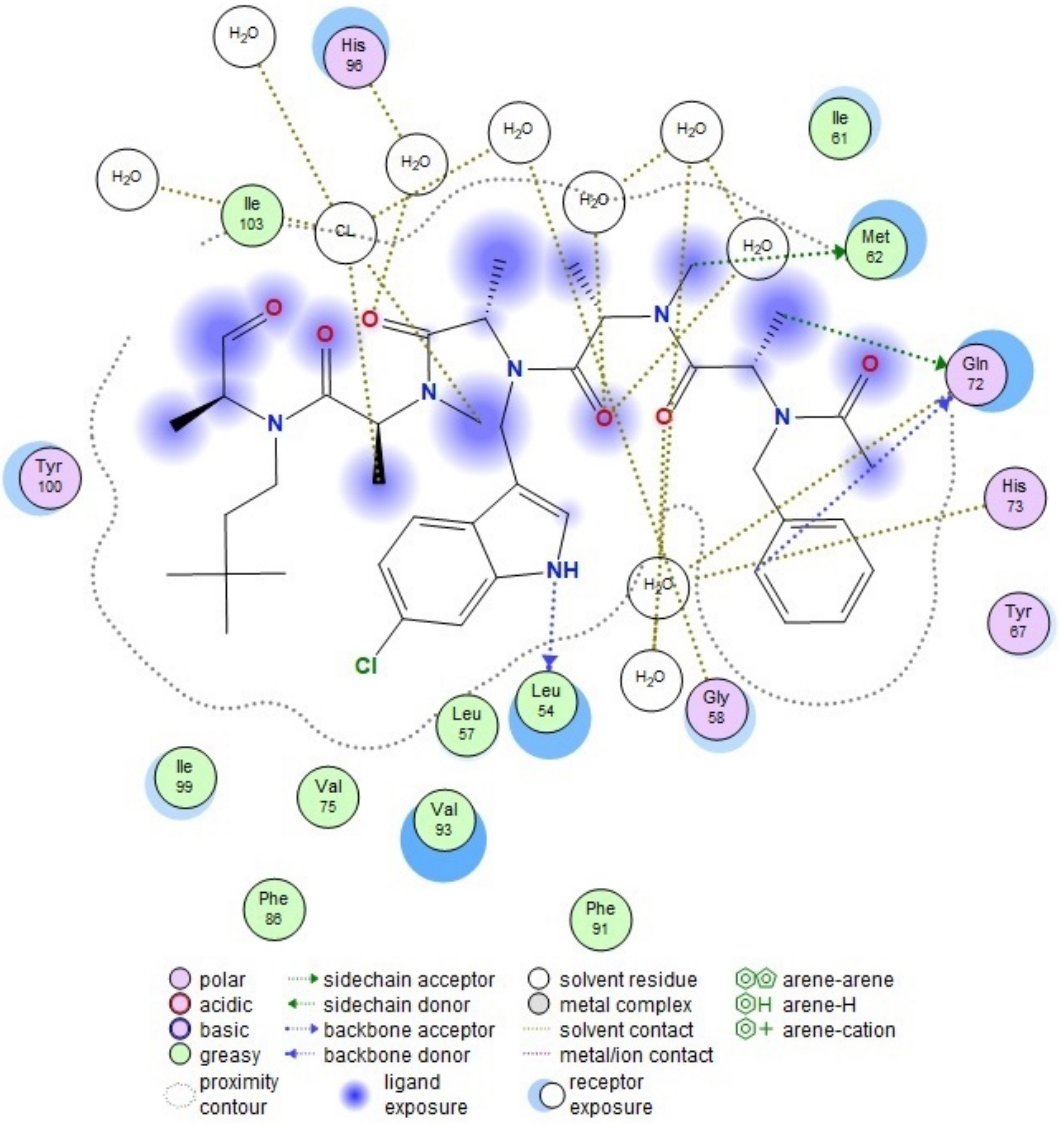

Fig. S1. 2D interactions map of the complex of **2** with MDM2 generated by the Ligand Interaction module in Molecular Operating Environment (MOE, Chemical Computing Group), showing all methyl groups on C_α are exposed to solvent.

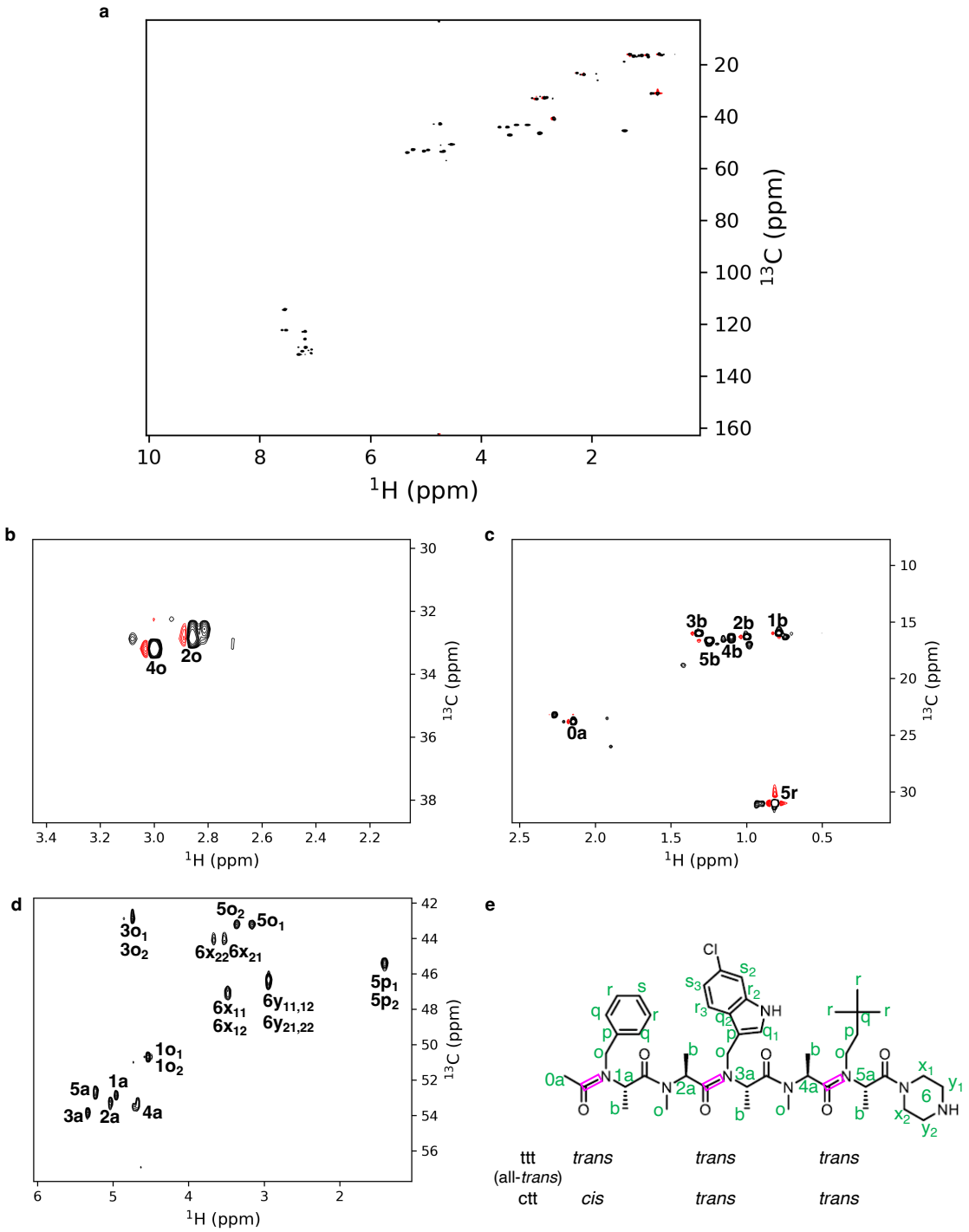

Fig. S2. (a–d) ^{1}H-^{13}C HSQC spectrum of **2** recorded in DMSO-d_6/D_2O = 20:80. *N*-Methyl, methyl, and H_α/*N*-methylene regions are enlarged in (b), (c), and (d) respectively. (e) Chemical structure of **2**. In (b–d), assignments are shown for the resonances in all-*trans* state. The resonance assignments are summarized in Table S3.

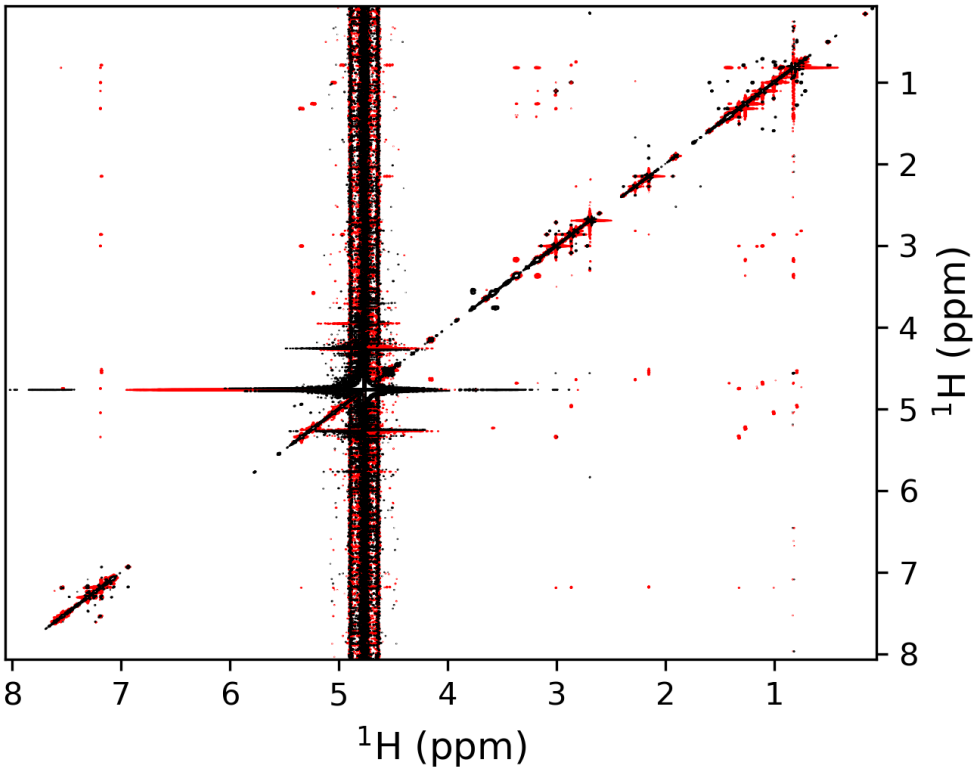

Fig. S3. EASY-ROESY spectrum of **2** recorded in DMSO-d_6/D_2O = 20:80.

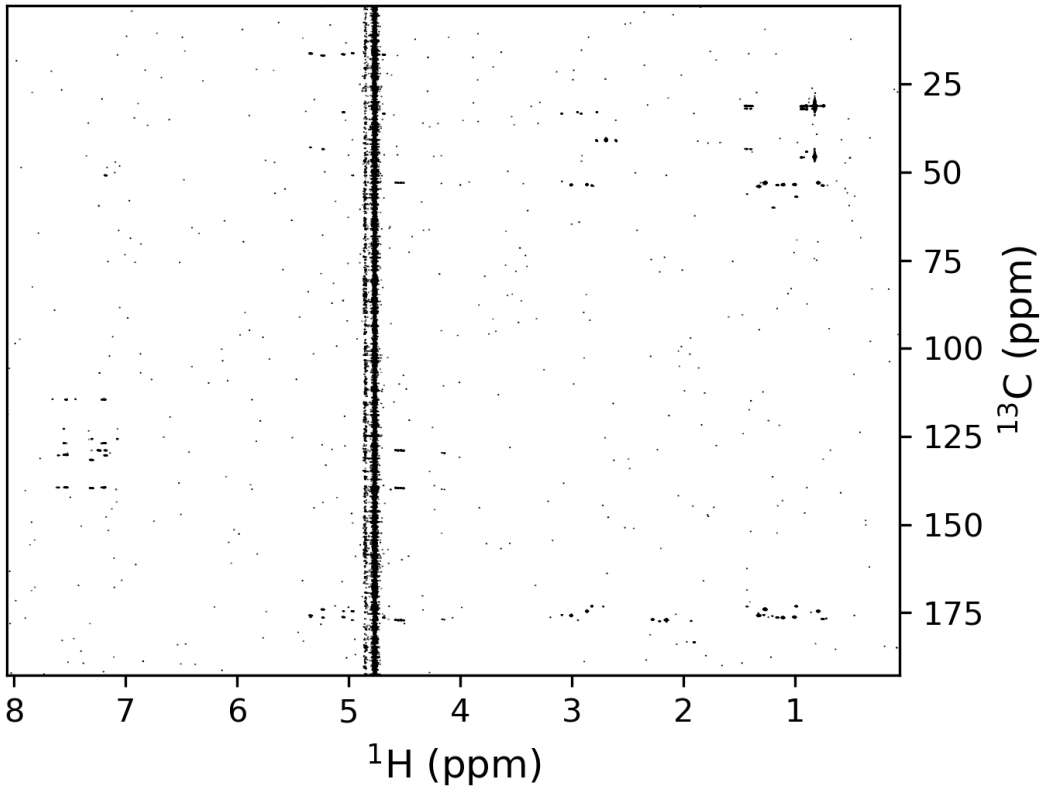

Fig. S4. ^{1}H-^{13}C HMBC spectrum of **2** recorded in DMSO-d_6/D_2O = 20:80. The resonance assignments are summarized in Table S3.

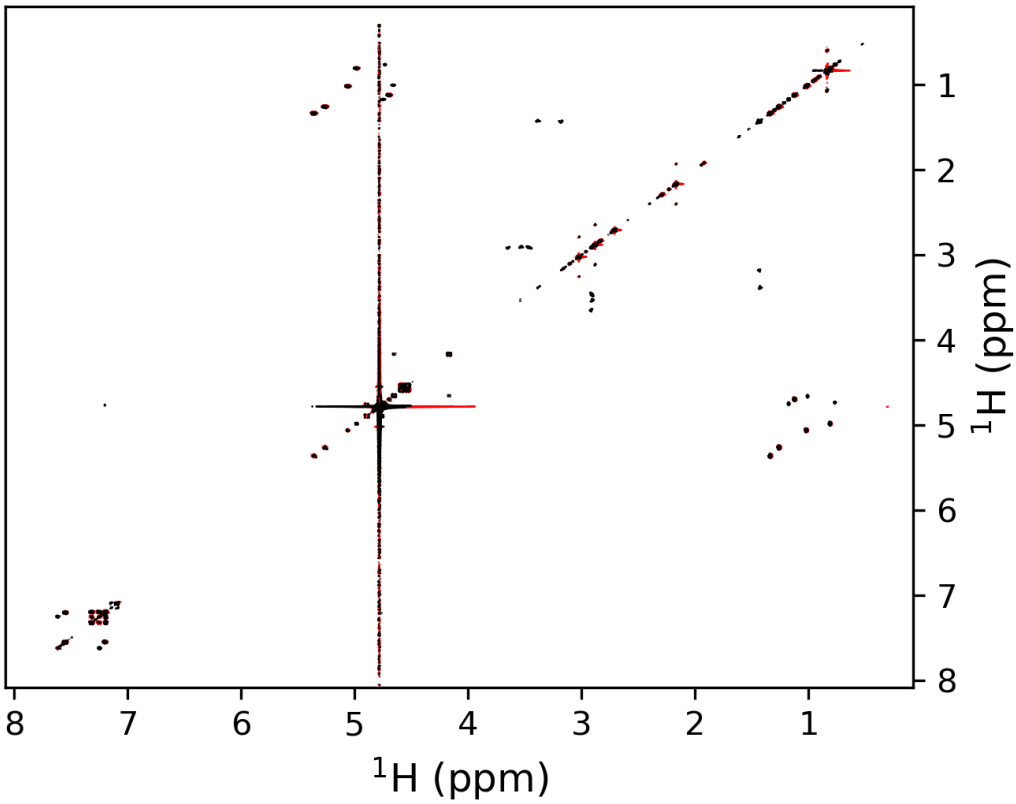

Fig. S5. TOCSY spectrum of **2** recorded in DMSO-d_6/D_2O = 20:80.

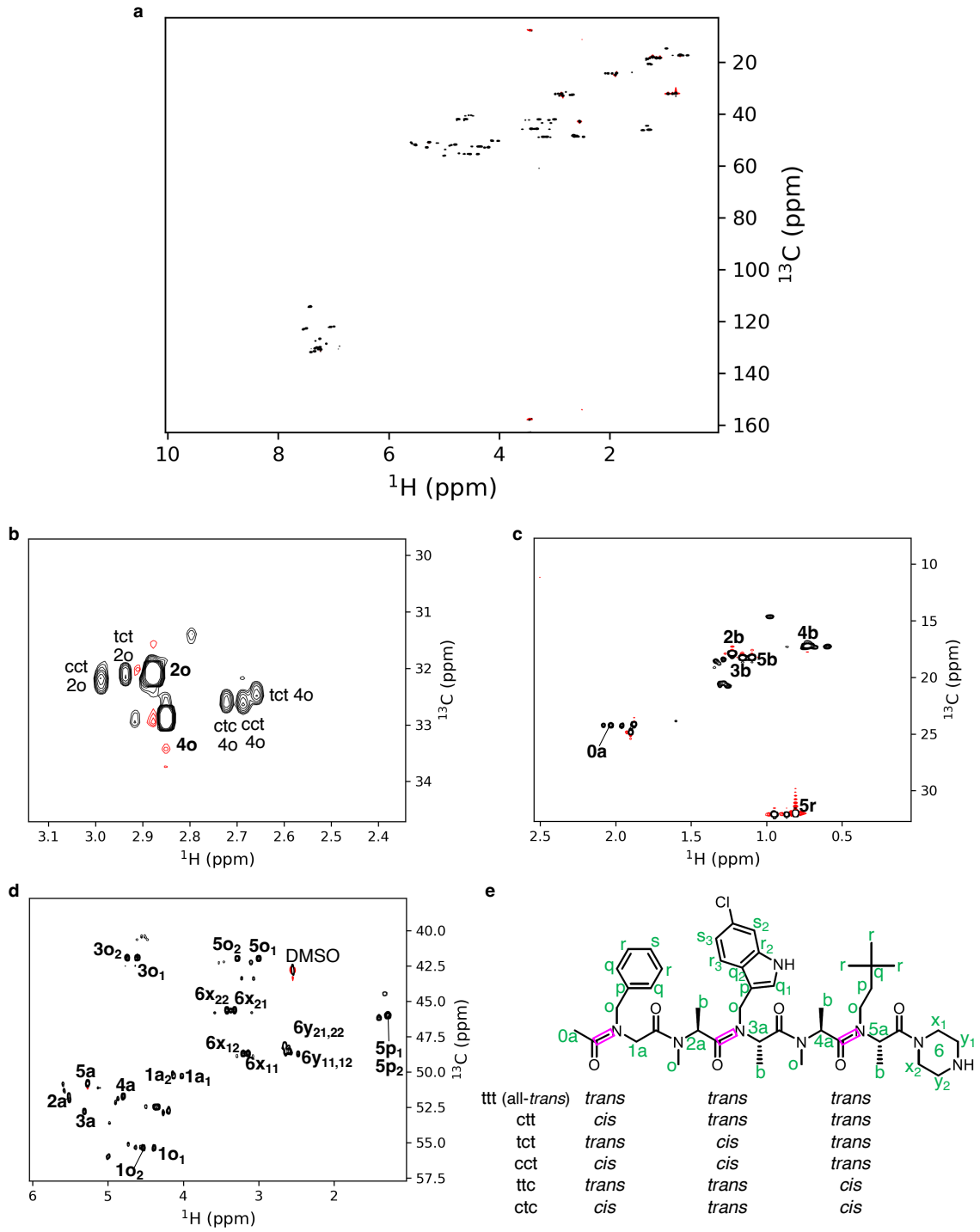

Fig. S6. (a–d) ^{1}H-^{13}C HSQC spectrum of **3** recorded in DMSO-*d*$_6$. *N*-Methyl, methyl, and H$_\alpha$/*N*-methylene regions are enlarged in (b), (c), and (d) respectively. In (b), resonances corresponding to the all-*trans* state are labeled with bold letters, and the *cis-trans* isomerization state of the other resonances are indicated. In (c,d), assignments are shown for the resonances in all-*trans* state. The resonance assignments are summarized in Table S4. Positive and negative signals are colored black and red, respectively. (e) Chemical structure of **3**. Peptide bonds that exhibited *cis-trans* equilibria were surrounded by magenta squares.

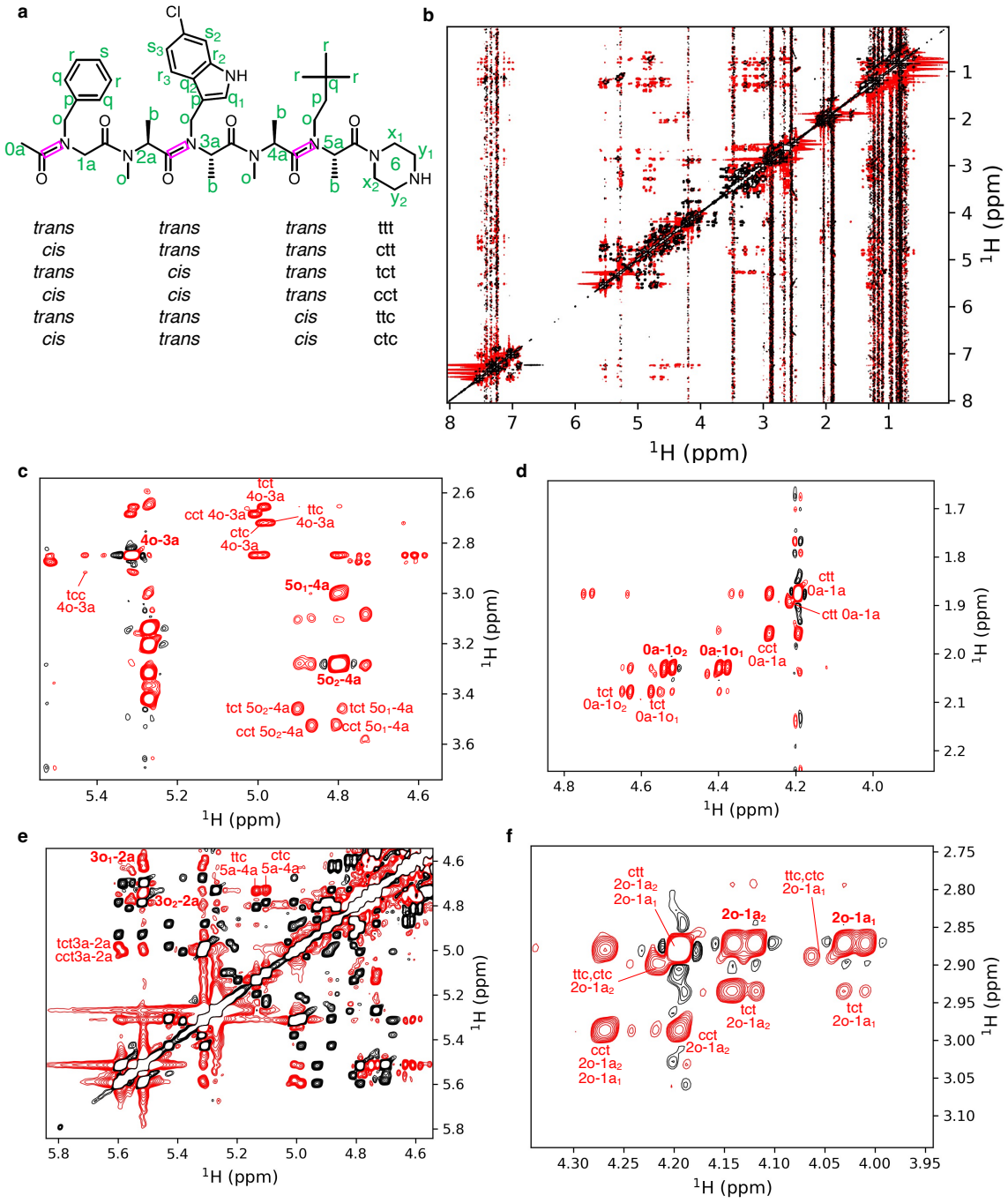

Fig. S7. (a) Chemical structure of **3**. Peptide bonds that exhibited *cis-trans* equilibria were surrounded by magenta squares. (b–e) EASY-ROESY spectrum of **3** recorded in DMSO-d_6. In (c–f), NOE signals that define the *cis-trans* isomerization state of the peptide bonds are enlarged. NOE signals of the all-*trans* state are labeled with bold letters, and the *cis-trans* isomerization state of the other resonances are indicated. The resonance assignments are summarized in Table S4. Positive and negative signals are colored black and red, respectively.

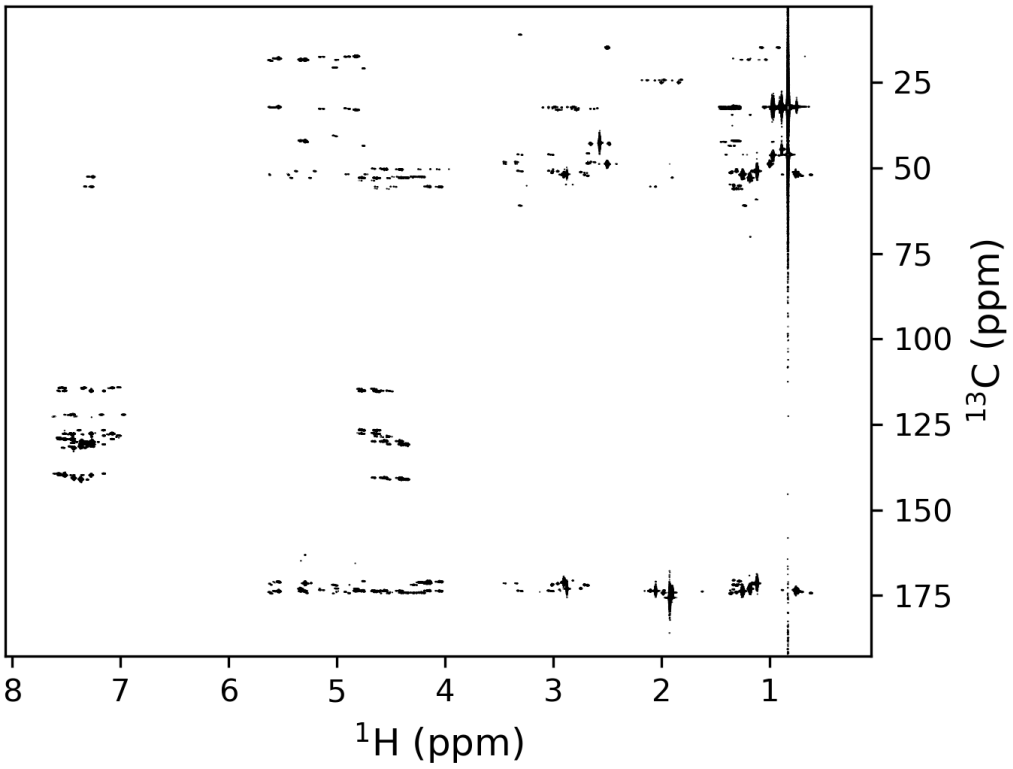

Fig. S8. ^{1}H-^{13}C HMBC spectrum of **3** recorded in DMSO-*d*$_6$. The resonance assignments are summarized in Table S4.

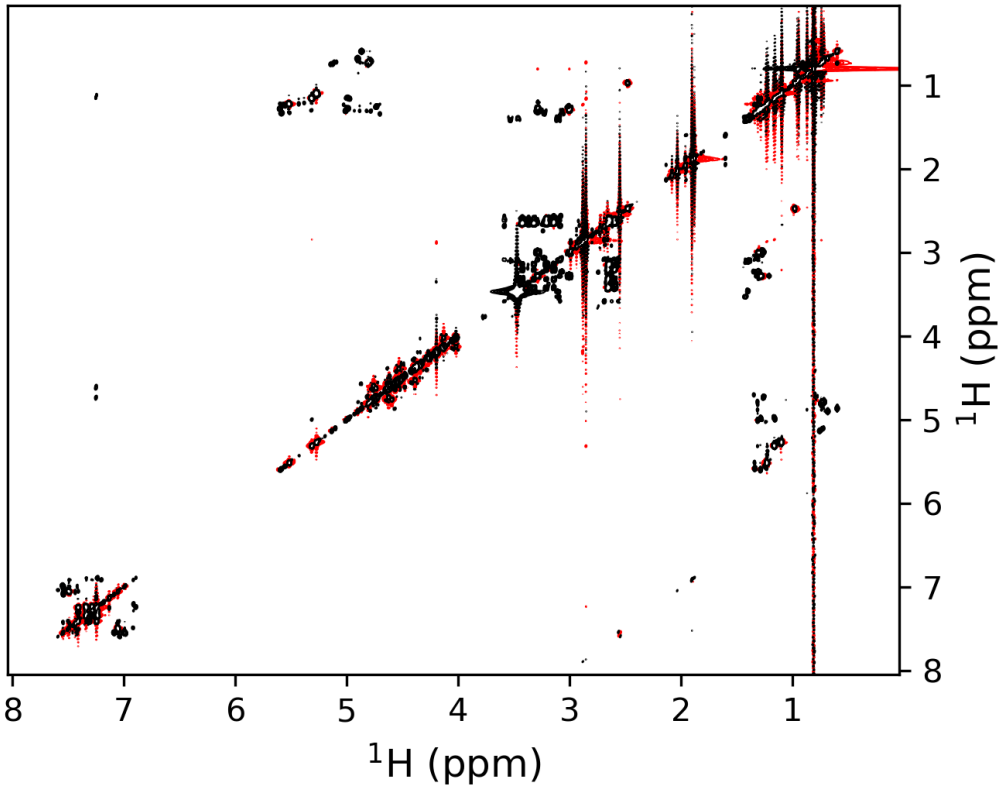

Fig. S9. TOCSY spectrum of **3** recorded in DMSO-*d*$_6$.

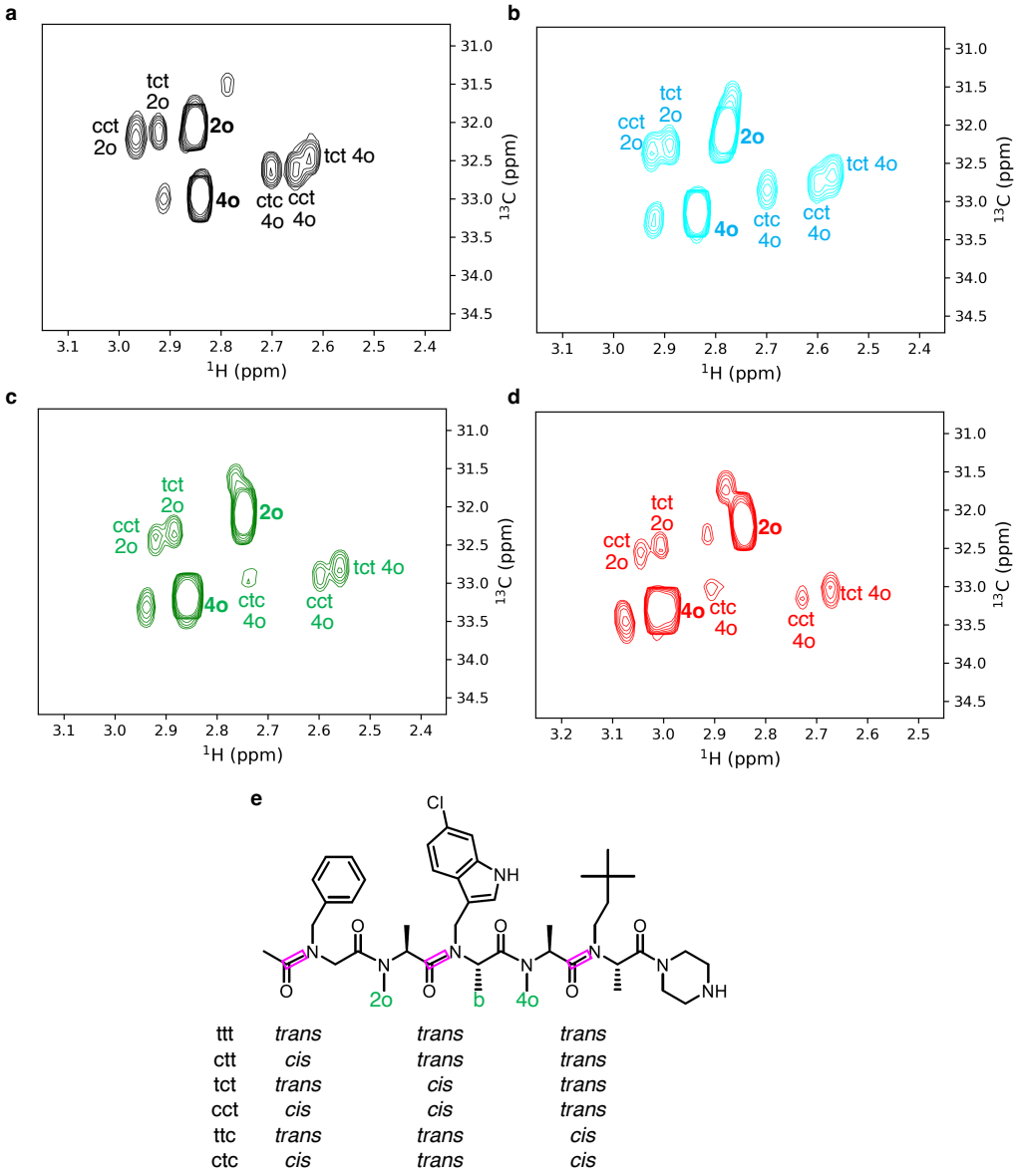

Fig. S10. *N*-Methyl region of the ^{1}H-^{13}C HSQC spectrum of **3** recorded in DMSO-*d*$_6$ (a, black), DMSO-*d*$_6$/D$_2$O = 2:1 (b, cyan), DMSO-*d*$_6$/D$_2$O = 1:1 (c, green), and DMSO-*d*$_6$/D$_2$O = 1:4 (d, red). Resonances corresponding to the all-*trans* state are labeled with bold letters, and the *cis*-*trans* isomerization state of the other resonances are indicated. (e) Chemical structure of **3**. Peptide bonds that exhibited *cis*-*trans* equilibria were surrounded by magenta squares.

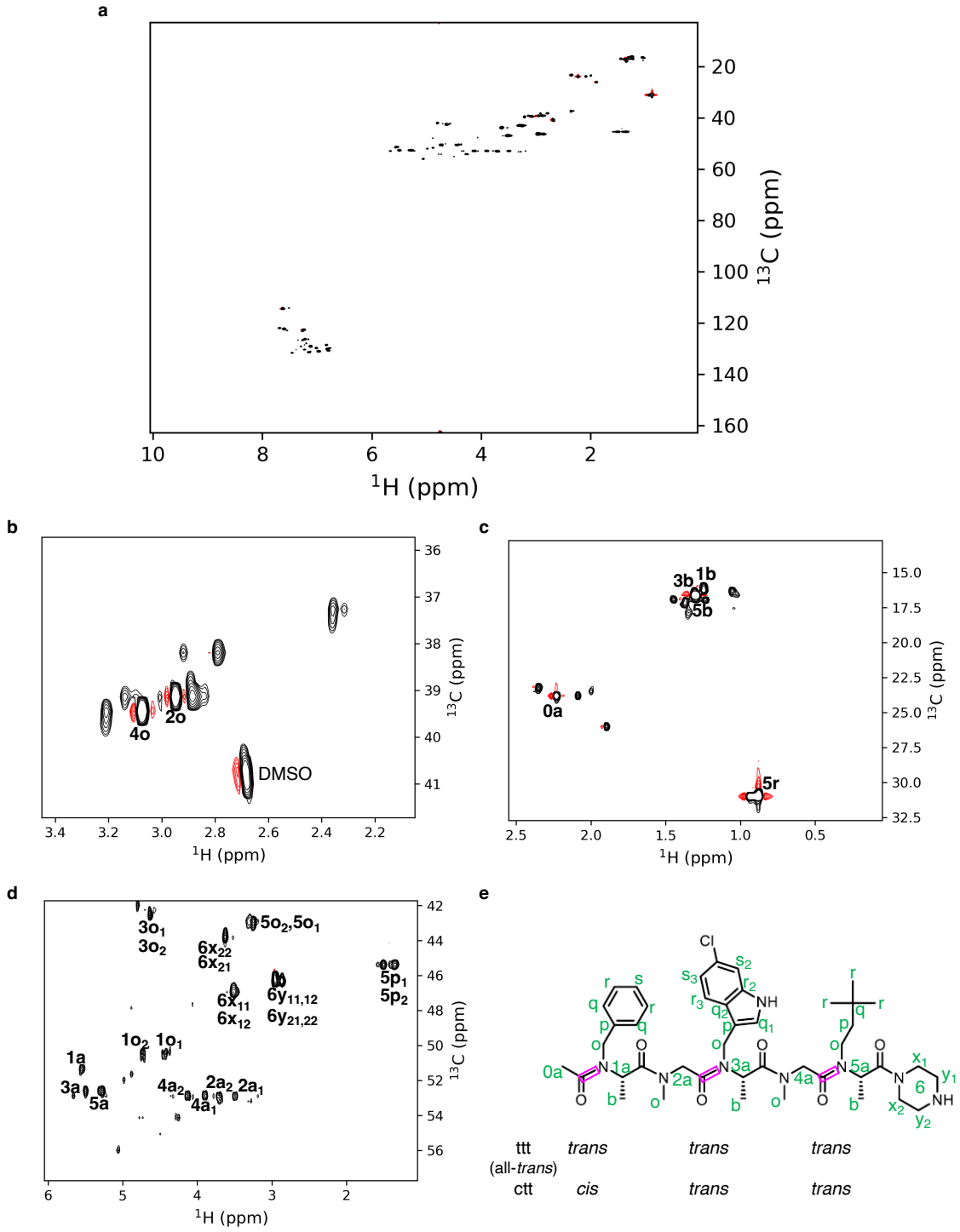

Fig. S11. (a–d) ^{1}H-^{13}C HSQC spectrum of **4** recorded in DMSO-*d*$_6$/D$_2$O = 20:80. *N*-Methyl, methyl, and H$_\alpha$/*N*-methylene regions are enlarged in (b), (c), and (d) respectively. (e) chemical structure of **4**. In (b–d), assignments are shown for the resonances in all-*trans* state. The resonance assignments are summarized in Table S5.

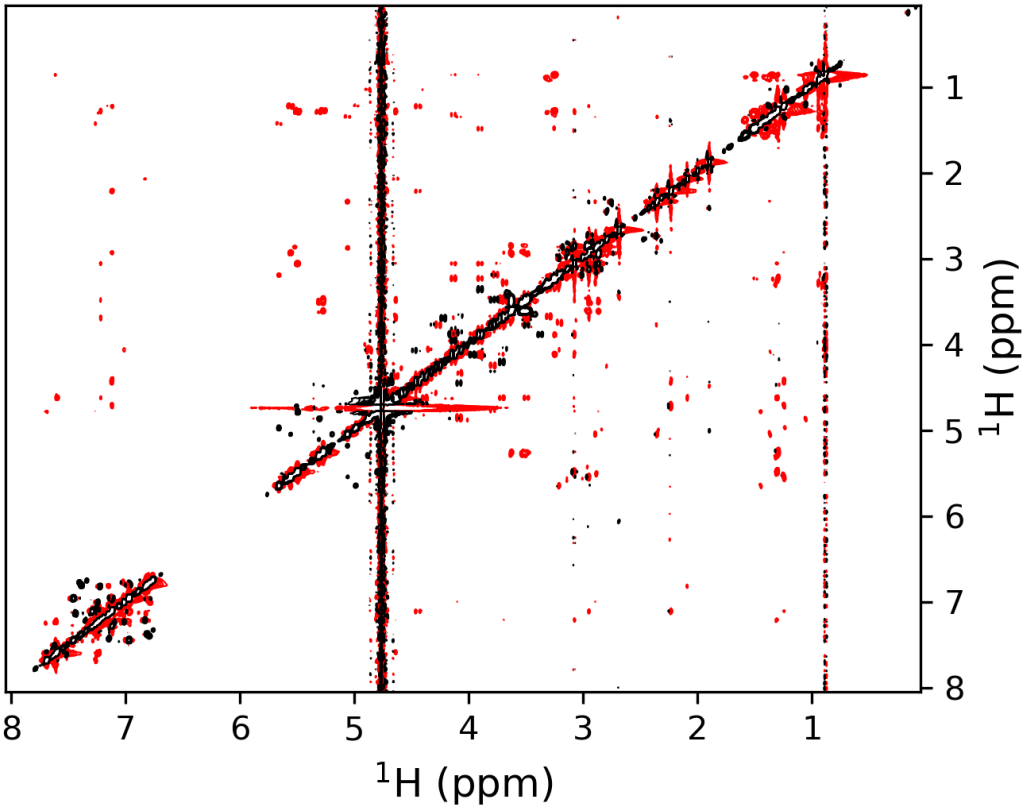

Fig. S12. EASY-ROESY spectrum of **4** recorded in DMSO-d_6/D_2O = 20:80.

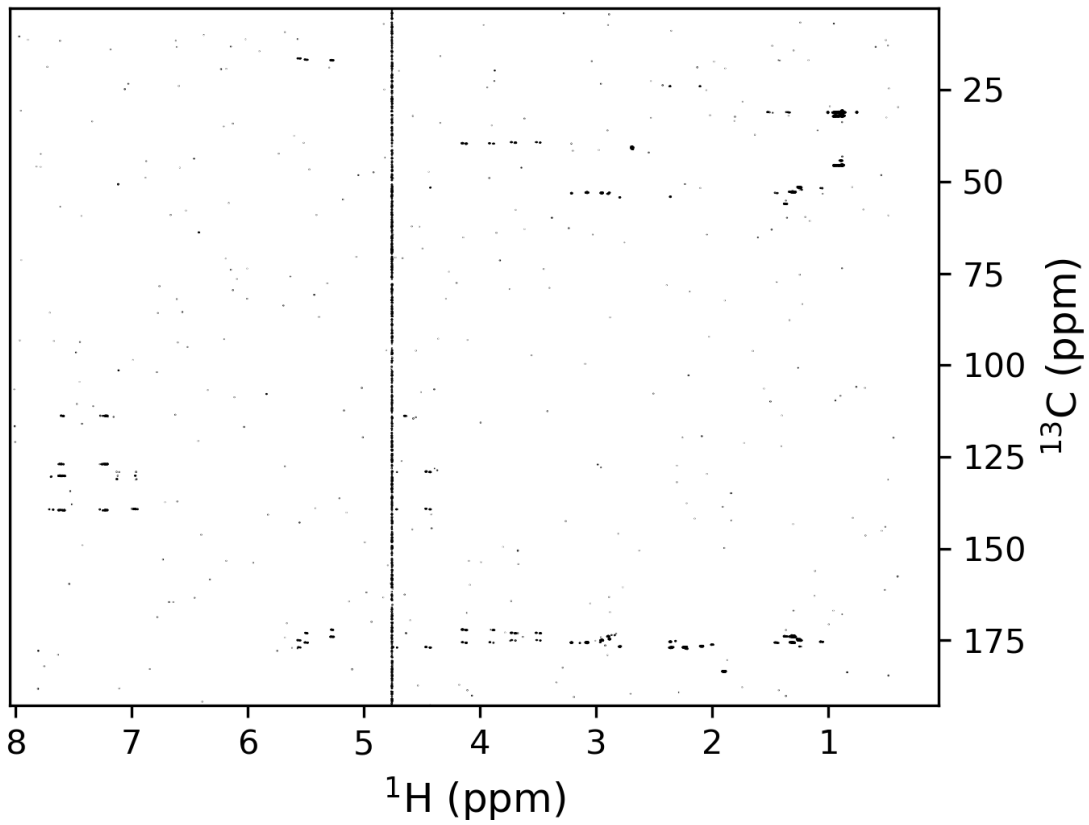

Fig. S13. ^{1}H-^{13}C HMBC spectrum of **4** recorded in DMSO-d_6/D_2O = 20:80. The resonance assignments are summarized in Table S5.

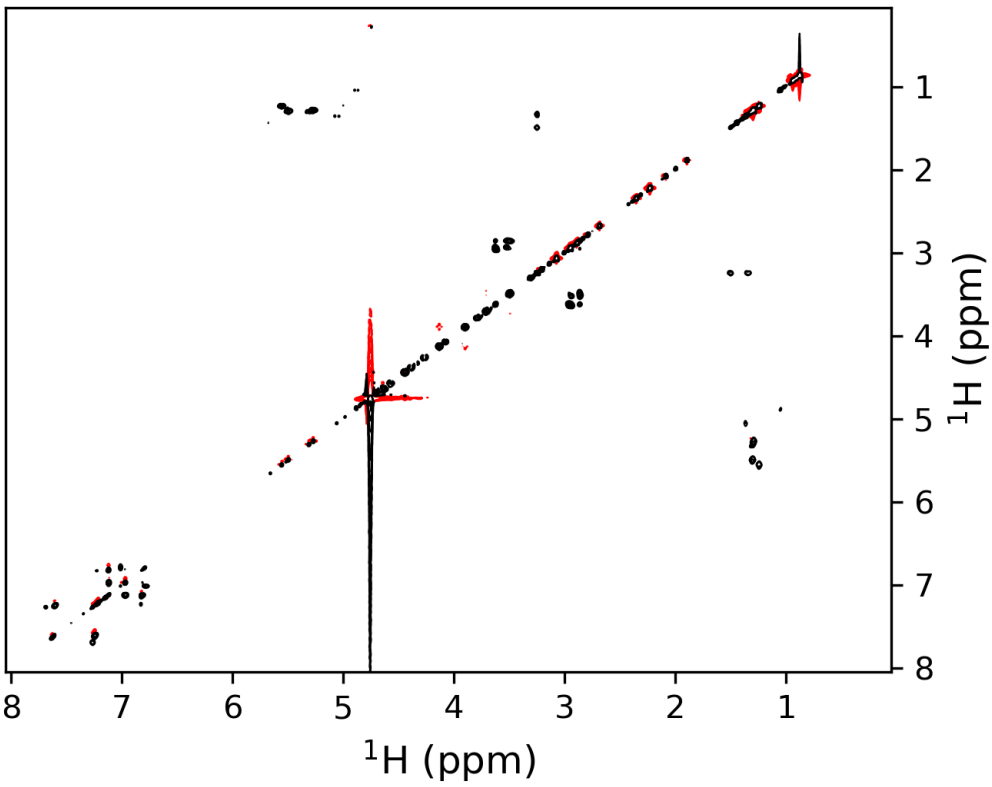

Fig. S14. TOCSY spectrum of **4** recorded in DMSO-d_6/D_2O = 20:80.

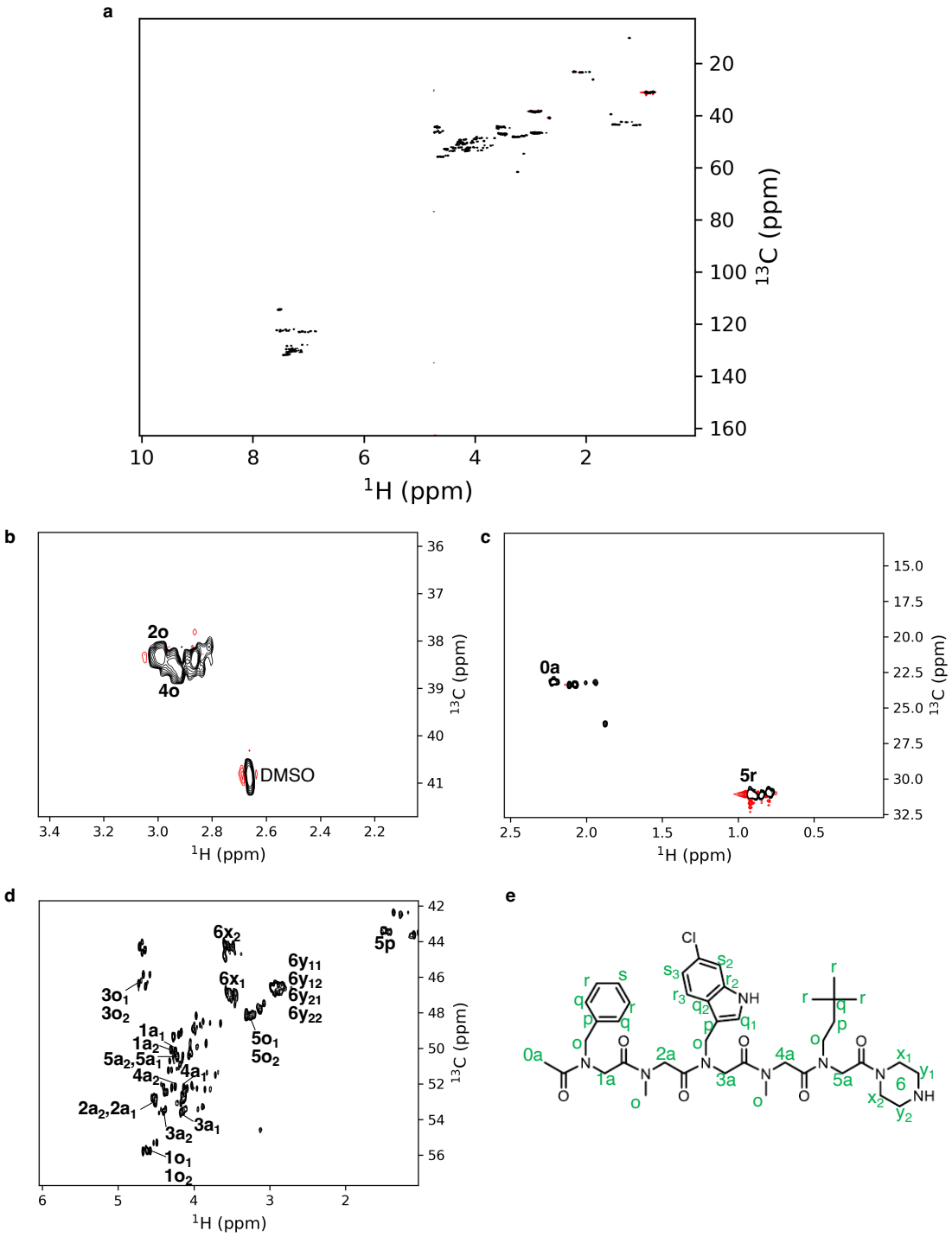

Fig. S15. (a–d) ^{1}H-^{13}C HSQC spectrum of **5** recorded in DMSO-d_6/D_2O = 20:80. *N*-Methyl, methyl, and H_α/*N*-methylene regions are enlarged in (b), (c), and (d) respectively. (e) chemical structure of **5**. In (b–d), assignments are shown for the resonances in all-*trans* state. The resonance assignments are summarized in Table S6.

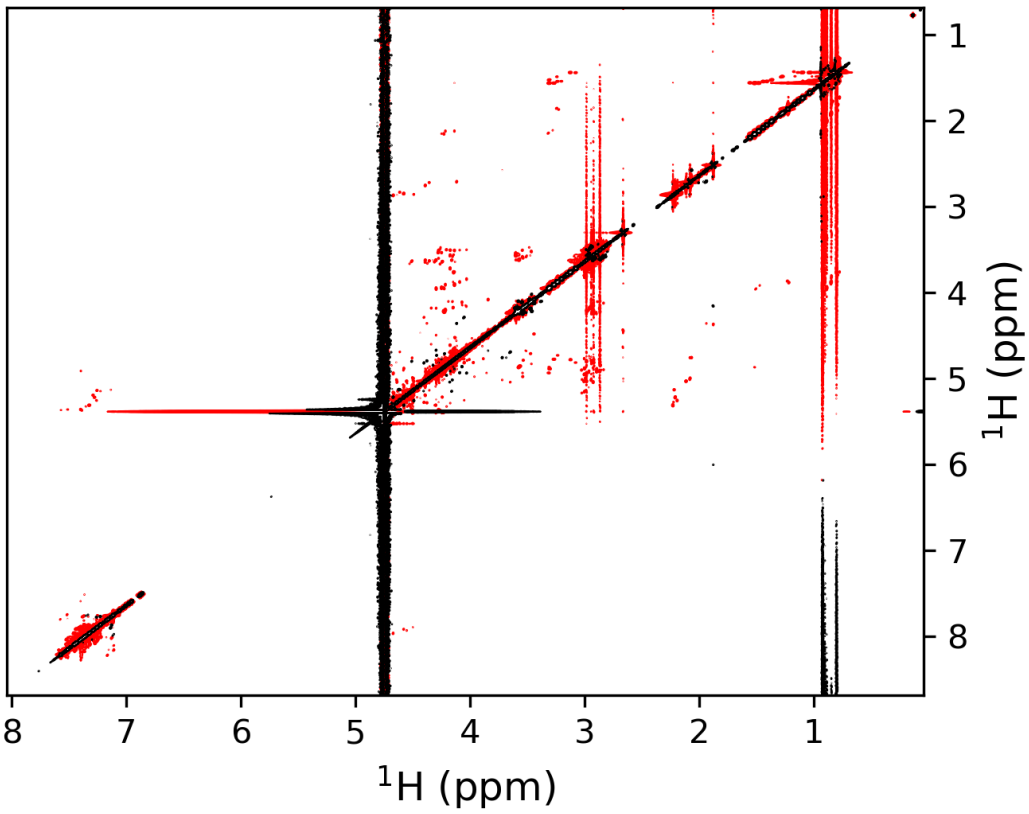

Fig. S16. EASY-ROESY spectrum of **5** recorded in DMSO-d_6/D_2O = 20:80.

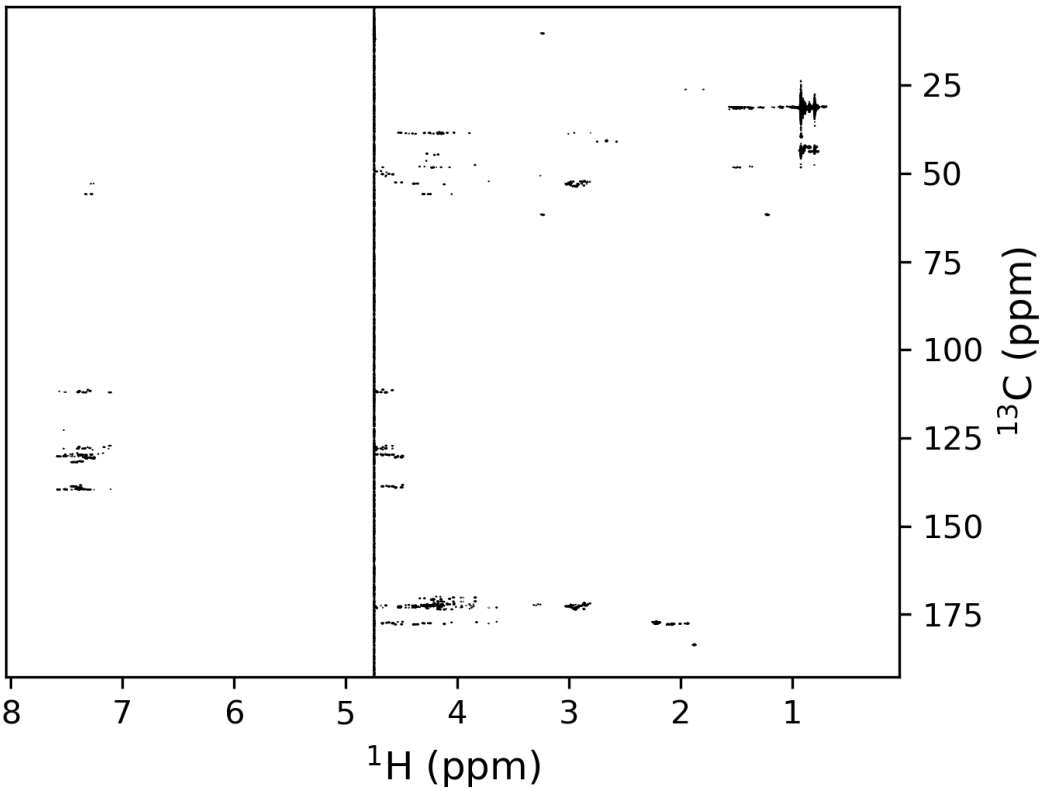

Fig. S17. ^{1}H-^{13}C HMBC spectrum of **5** recorded in DMSO-*d*$_6$/D$_2$O = 20:80.

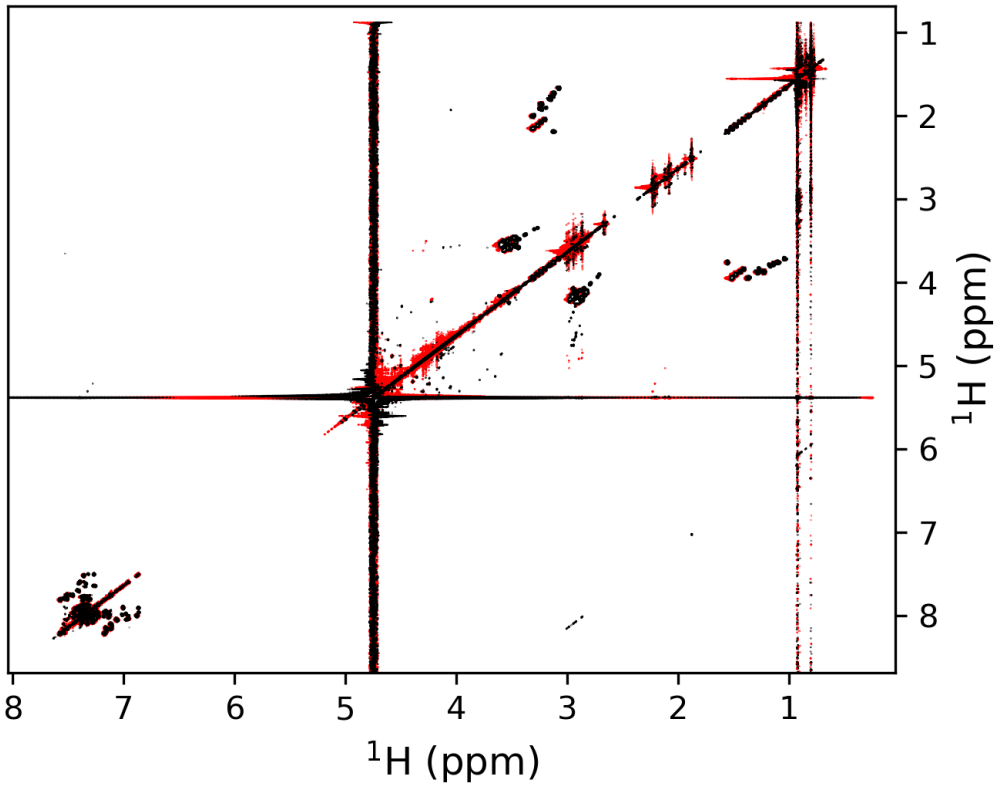

Fig. S18. TOCSY spectrum of **5** recorded in DMSO-d_6/D_2O = 20:80.

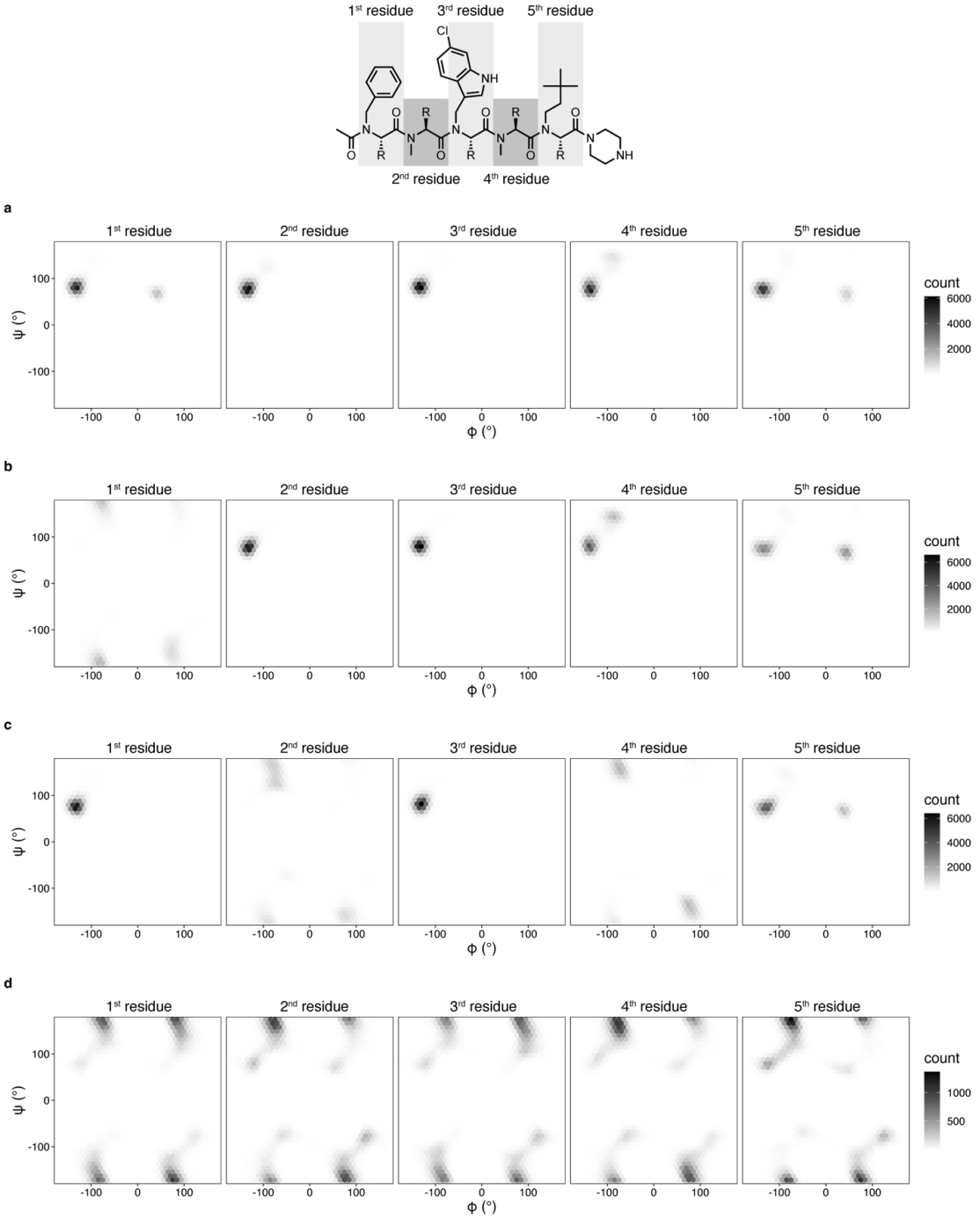

Fig. S19. Distribution of φ and ψ angles of (a) **2**, (b) **3**, (c) **4**, and (d) **5** during molecular dynamics (MD) simulations. The results of Run1–5 are integrated into a single plot.

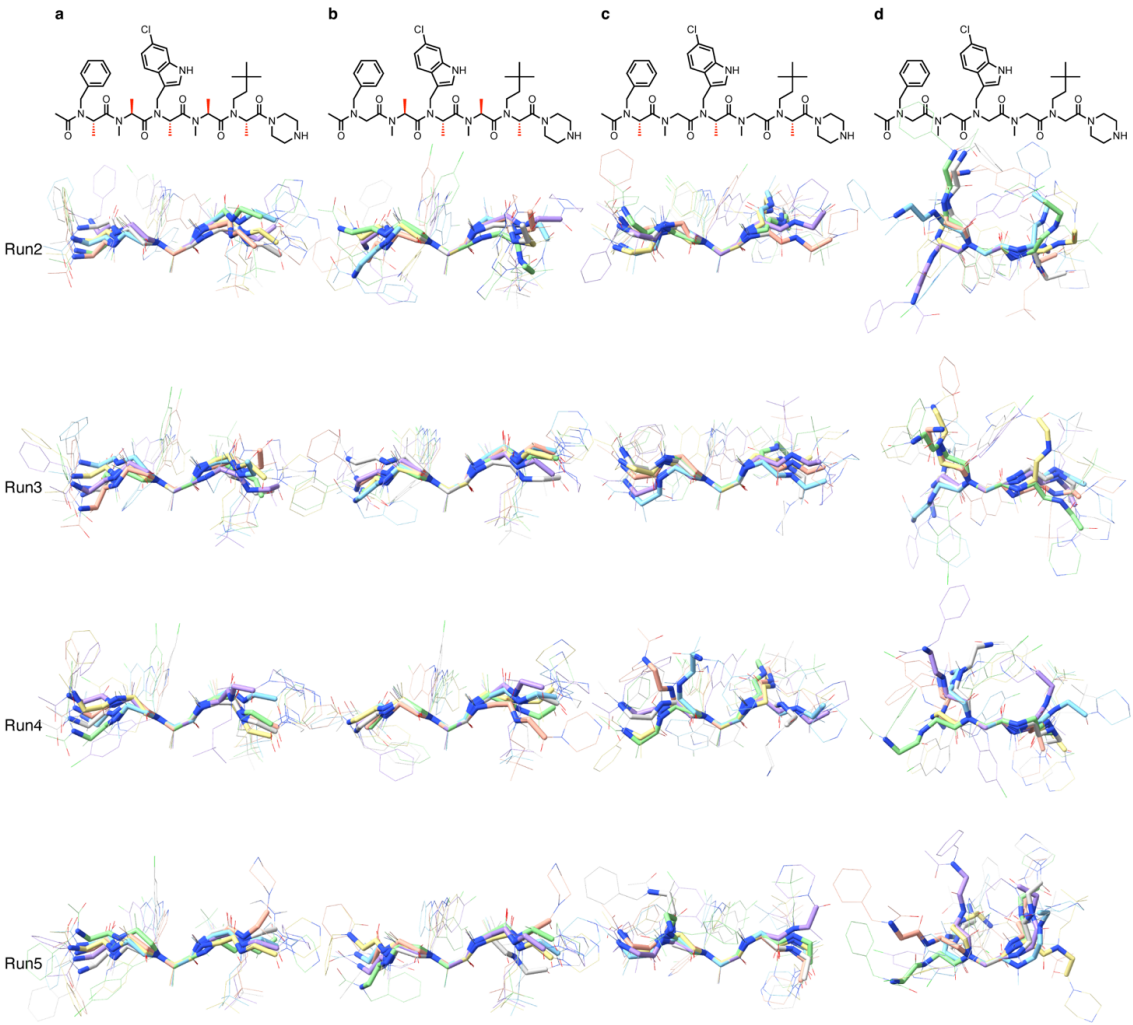

Fig. S20. Conformations of (a) **2**, (b) **3**, (c) **4**, and (d) **5** at every 100 ns during MD simulations. The conformations from each run are overlaid by N, C_α, and C of the third residue (violet = 0 ns, cyan = 100 ns, pink = 200 ns, light green = 300 ns, yellow = 400 ns, gray = 500 ns).

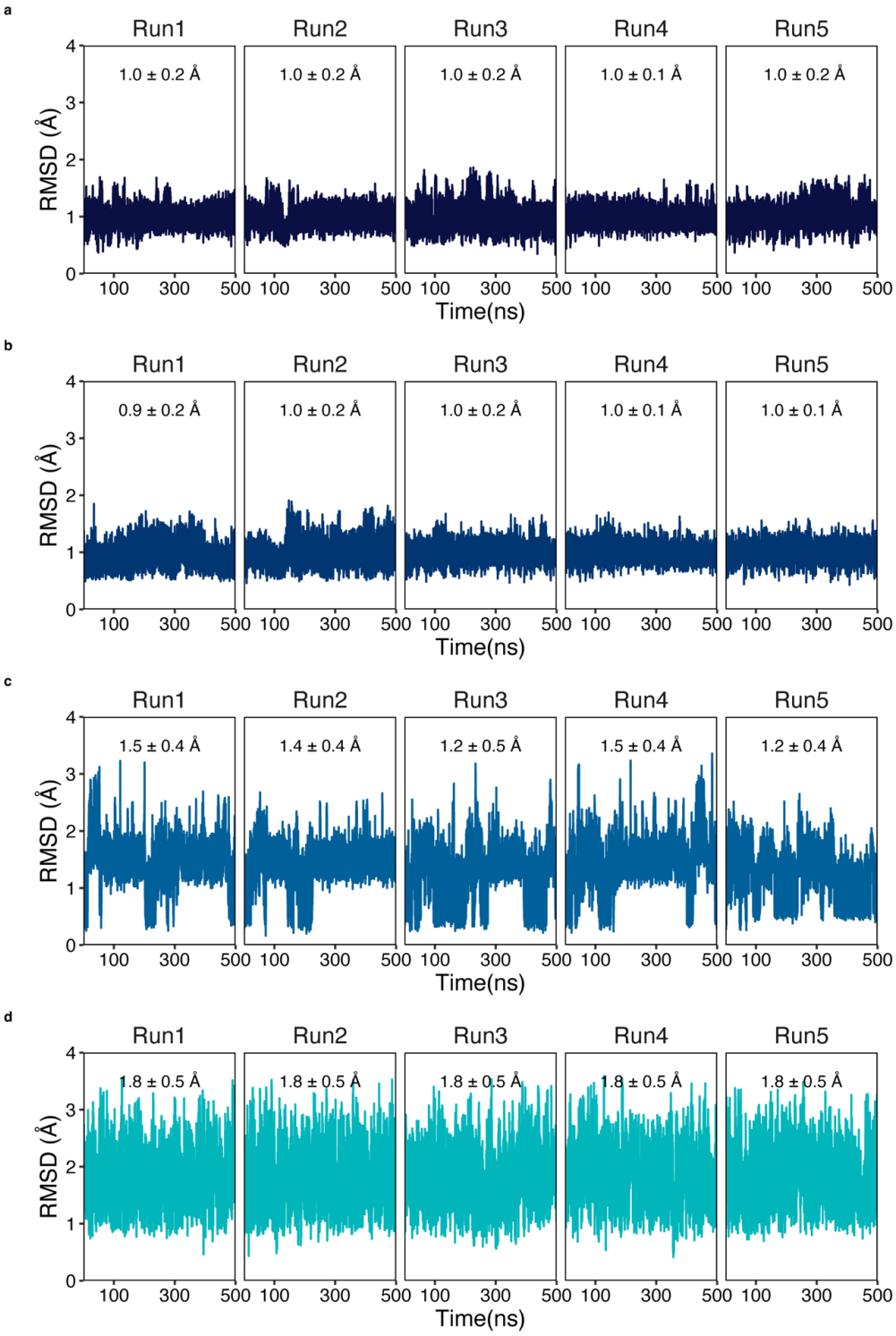

Fig. S21. Root-mean-square deviation (RMSD) values of backbone atoms (N, C_α, C) of (a) **2**, (b) **3**, (c) **4**, and (d) **5** compared to the crystal structure during MD simulations of peptoids.

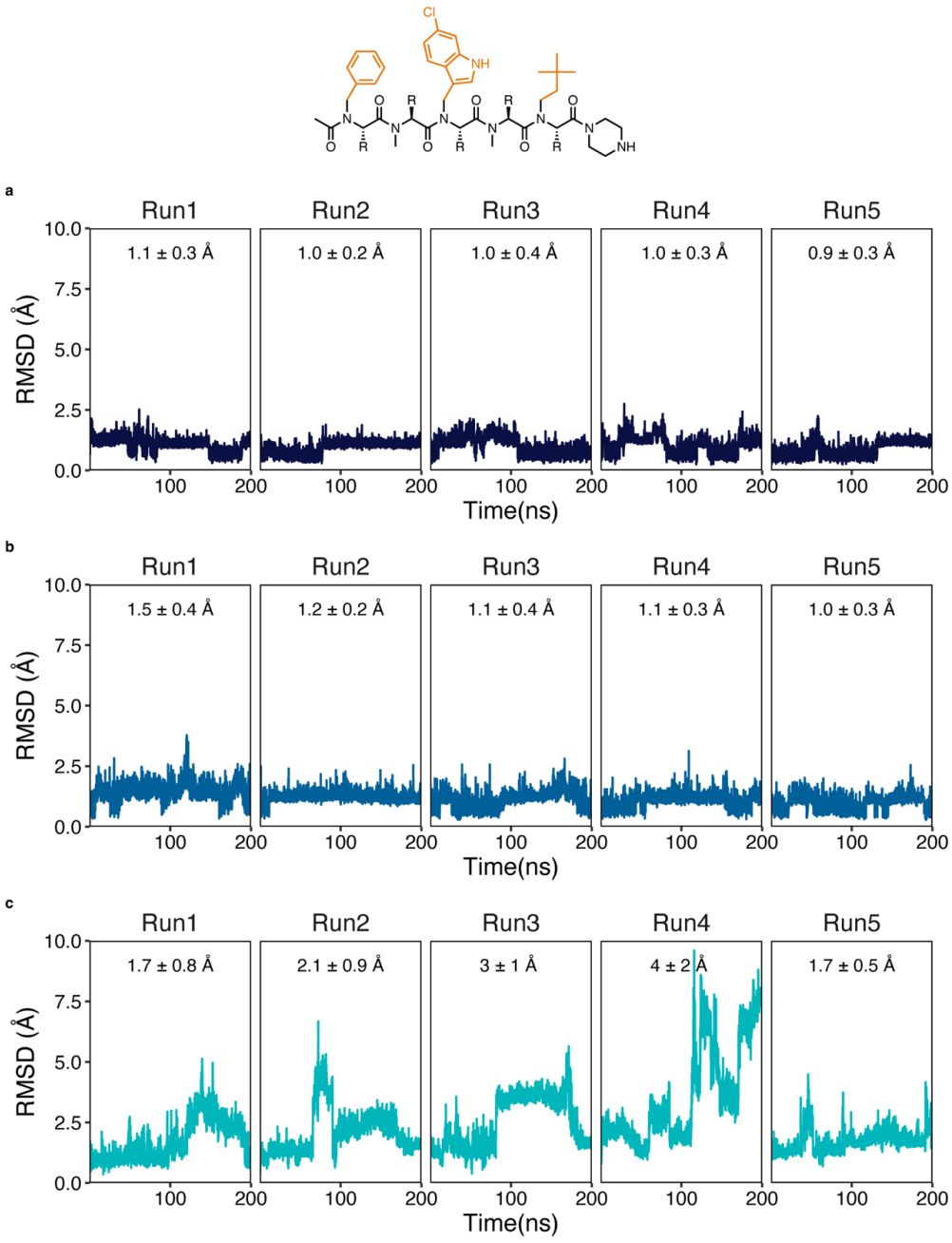

Fig. S22. RMSD values of side-chain atoms (orange) of (a) **2**, (b) **4**, and (c) **5** compared to the crystal structure fitted by C_α of MDM2 during MD simulations of peptoids in complex with MDM2.

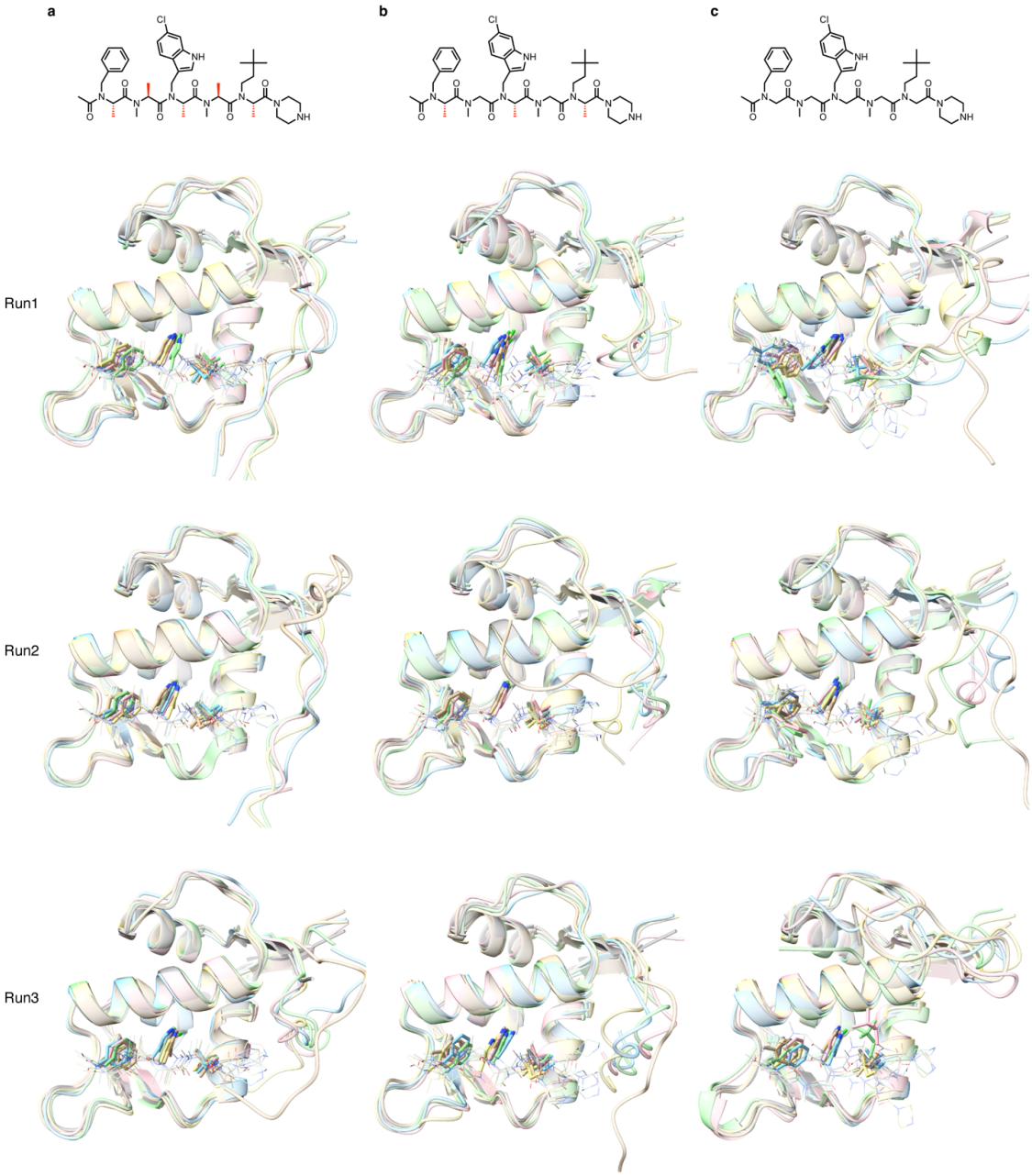

Fig. S23. Conformations of (a) **2**, (b) **4**, and (c) **5** in complex with MDM2 at every 50 ns during MD simulations. The conformations from each run and the crystal structure are overlaid by C_α of MDM2 (beige = 0 ns, cyan = 50 ns, pink = 100 ns, light green = 150 ns, yellow = 200 ns, gray = the crystal structure).

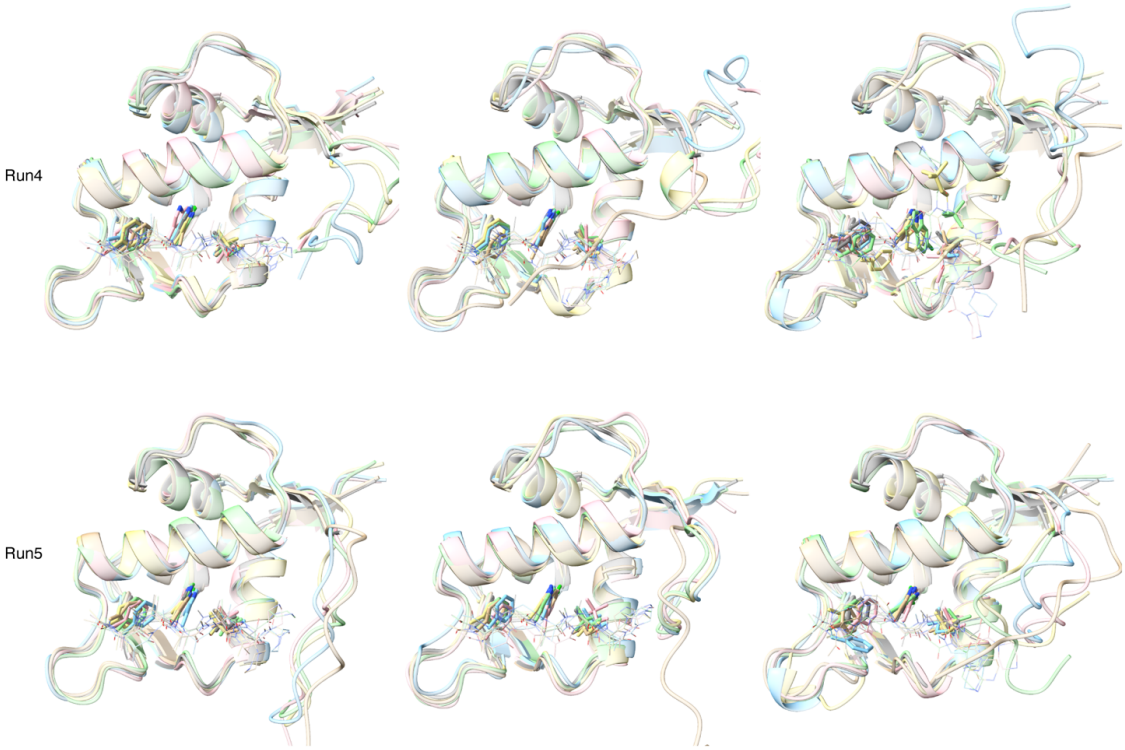

Continued.

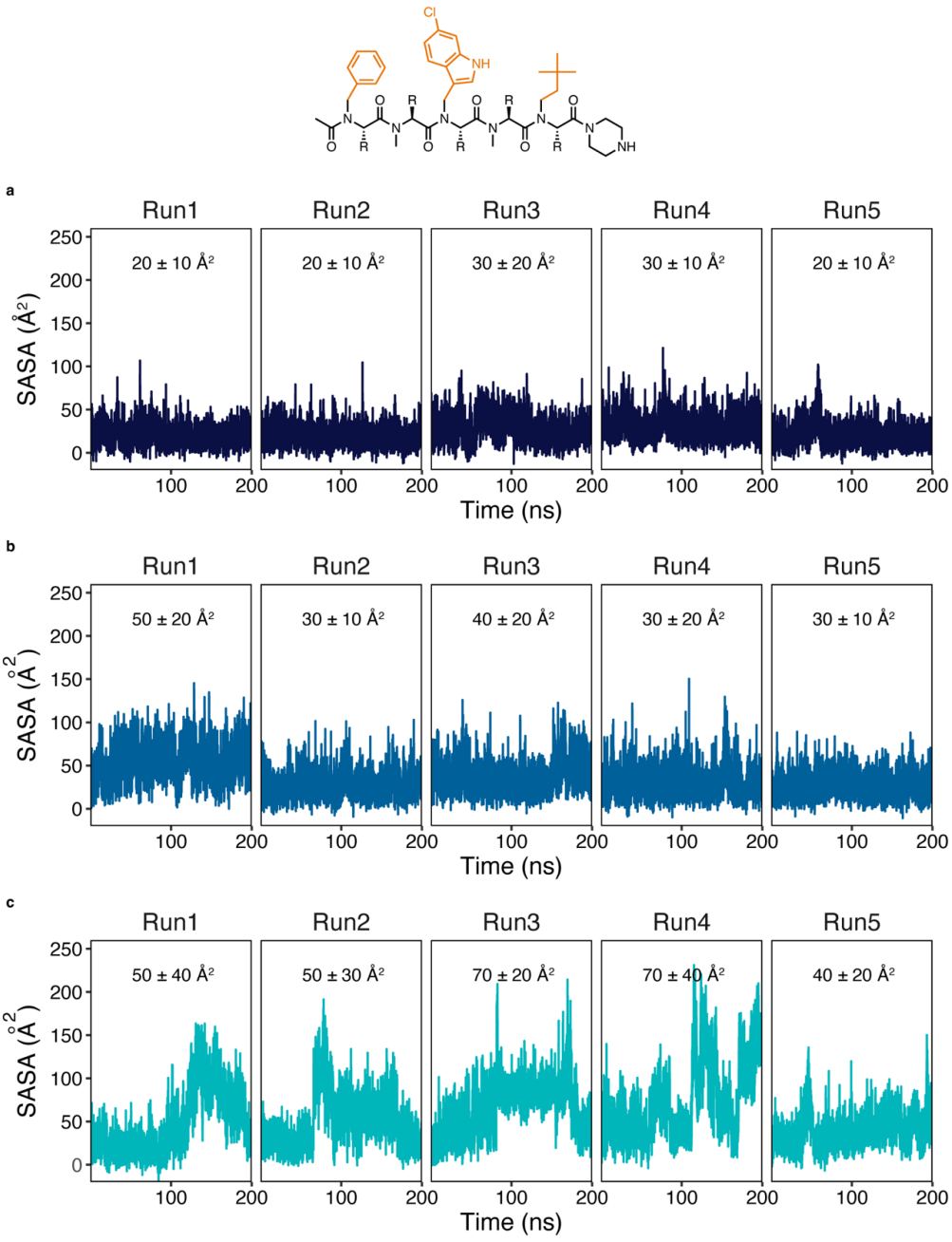

Fig. S24. Solvent accessible surface area (SASA) of side-chain atoms (orange) of (a) **2**, (b) **4**, and (c) **5** in complex with MDM2 during MD simulations.

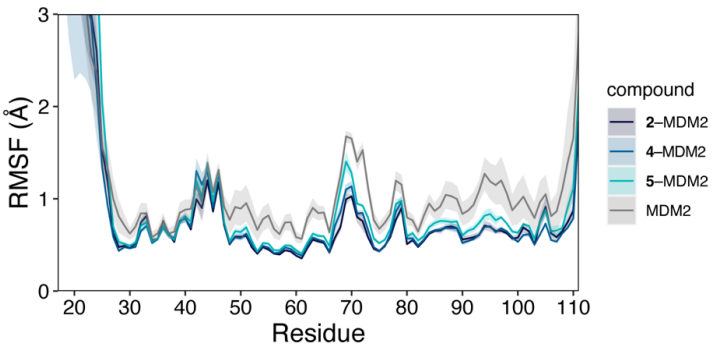

Fig. S25. RMSF values of MDM2 residues during MD simulations of MDM2 alone and MDM2 complexed with **2**, **4**, or **5**.

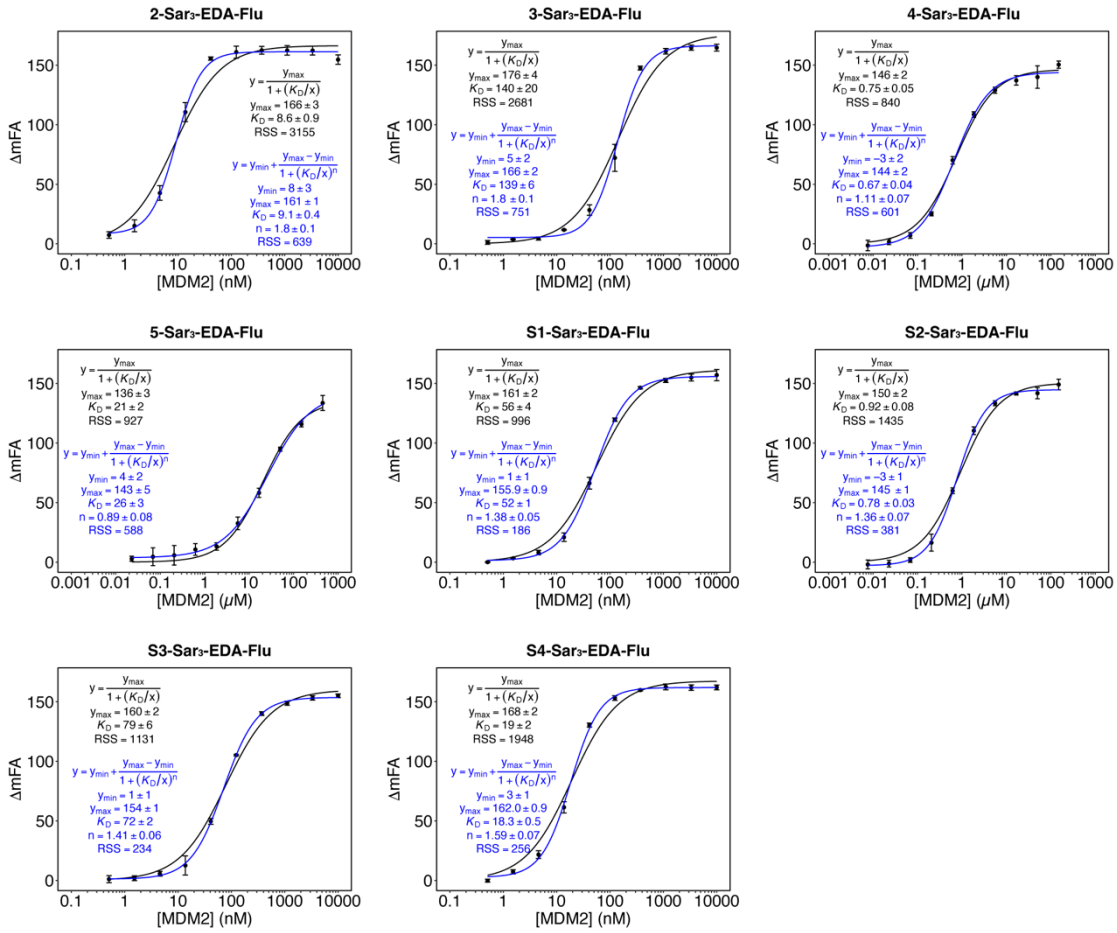

Fig. S26. Binding curves of peptoids with fluorescein-labeled ethylenediamine C-termini generated from an FA assay. Error bars represent standard deviations of triplicates. Parameters obtained from the curve fitting (Hill equation: $y = y_{min} + (y_{max} - y_{min})/(1 + (K_D/x)^n)$) of the acquired data are shown in blue in the graph. Parameters and binding curves shown in black are the result of fitting with n fixed at 1 and y_{min} fixed at 0, assuming the binding stoichiometry of 1:1. RSS means the residual sum of squares of the fitted model.

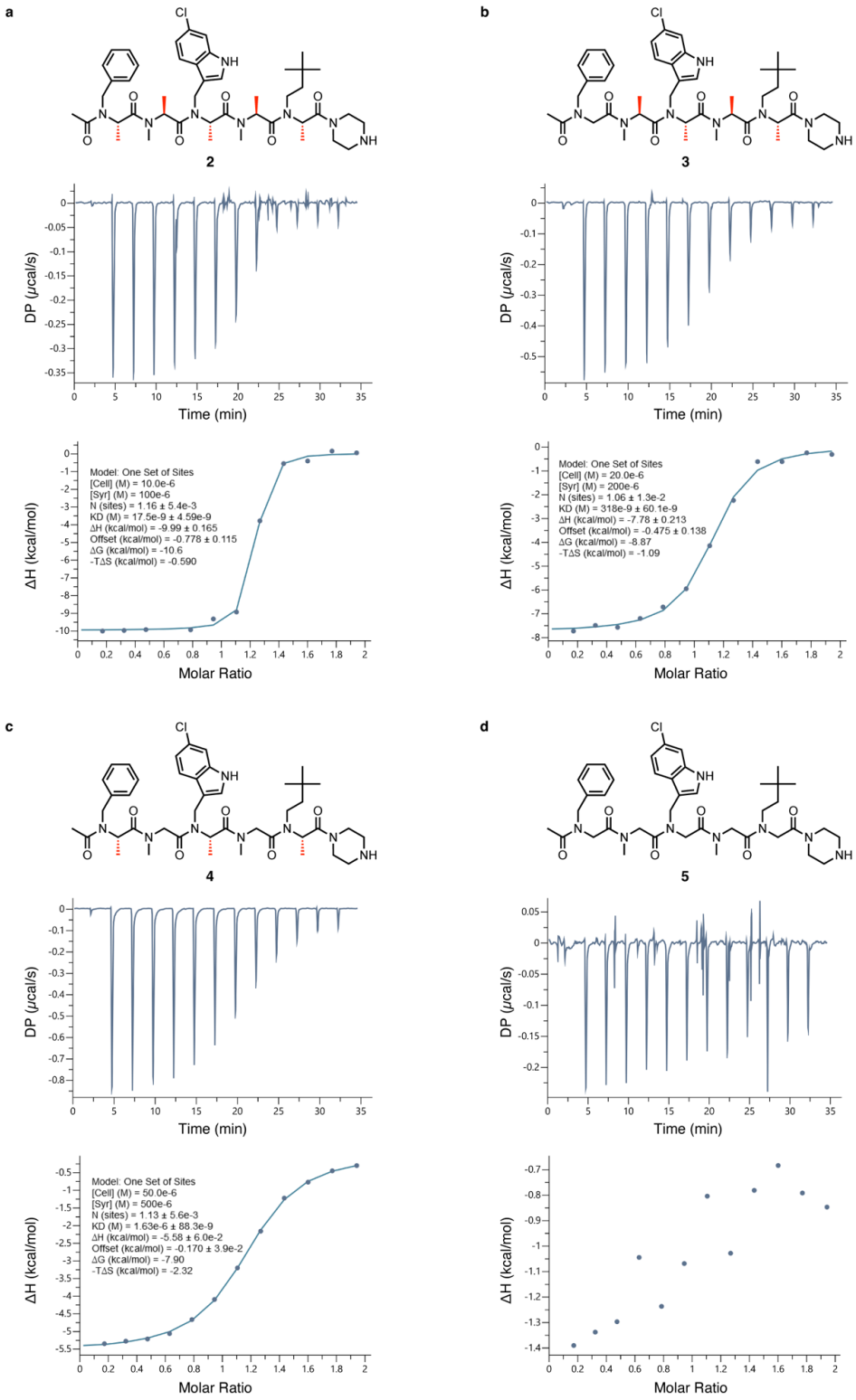

Fig. S27. Isothermal calorimetry data of binding of peptoids to MDM2. Isothermal calorimetry data of (a) **2**, (b) **3**, (c) **4** and (d) **5**. For (a–c), full parameters obtained from the fittings are shown. All the binding assays were conducted in PBS.

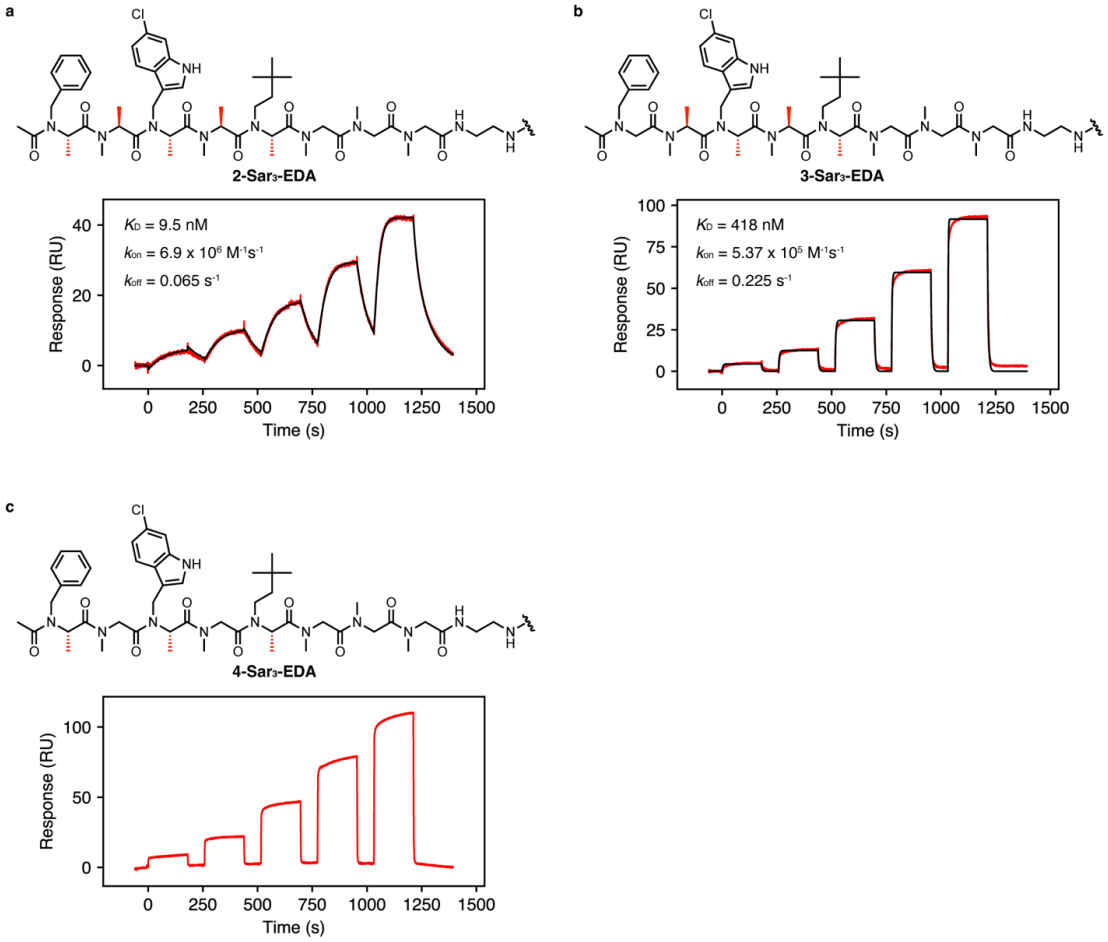

Fig. S28. Binding kinetics of peptoids to MDM2 measured by surface plasmon resonance (SPR) spectroscopy using Biacore T100. MDM2 was injected onto (a) **2-Sar$_3$-EDA**, (b) **3-Sar$_3$-EDA**, or (c) **4-Sar$_3$-EDA** immobilized CM5-chip (10 °C, running buffer: PBS (pH 7.4) containing 0.01% Tween 20, flow rate = 30 µL/min, contact time: 3 min, final dissociation time: 3 min). The sensorgrams of (a) and (b) were fitted to a 1:1 binding model. Shown in red is the raw data and in black is the data fit.

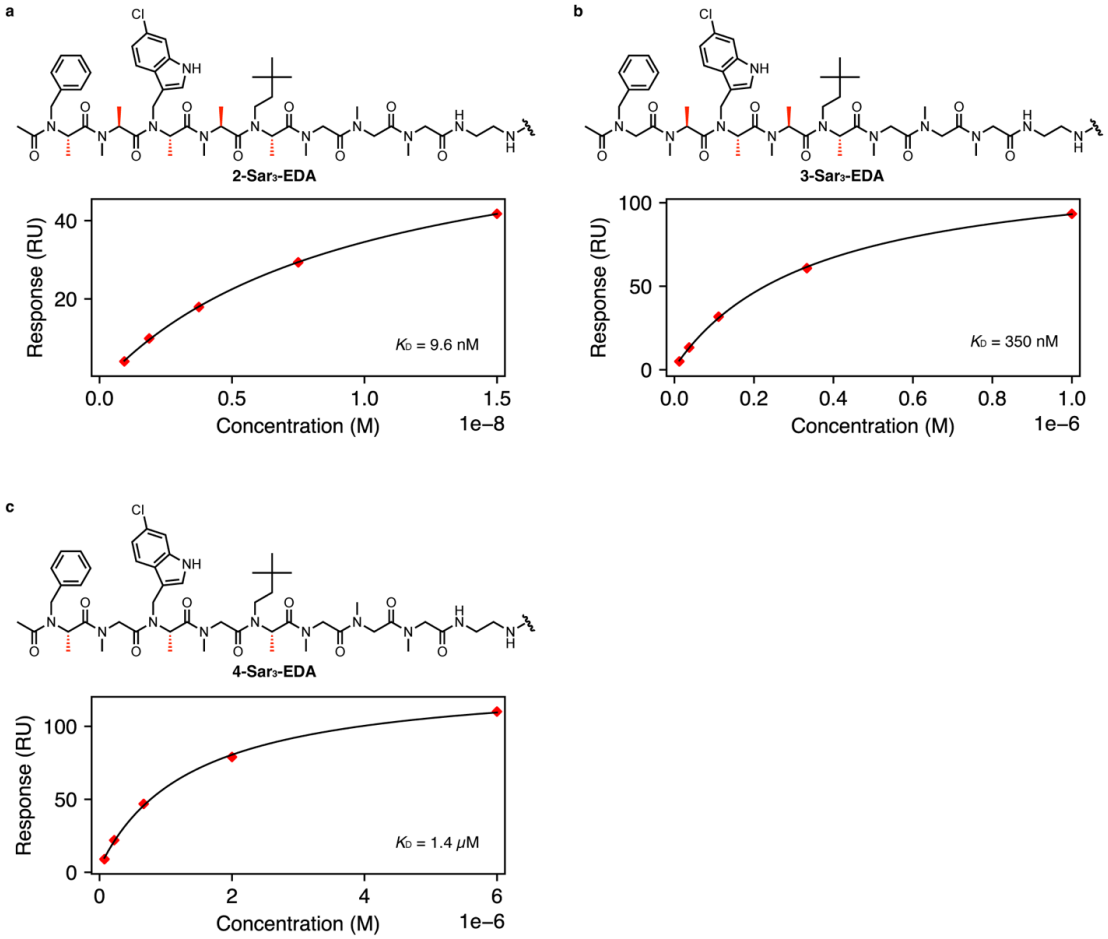

Fig. S29. Binding affinities of peptoids to MDM2 measured by SPR spectroscopy using Biacore T100. MDM2 was injected onto (a) **2-Sar$_3$-EDA**, (b) **3-Sar$_3$-EDA**, or (c) **4-Sar$_3$-EDA** immobilized CM5-chip (10 °C, running buffer: PBS (pH 7.4) containing 0.01% Tween 20, flow rate = 30 μL/min, contact time: 3 min, final dissociation time: 3 min). The plots were fitted to a steady-state affinity model. Shown in red is the raw data and in black is the data fit.

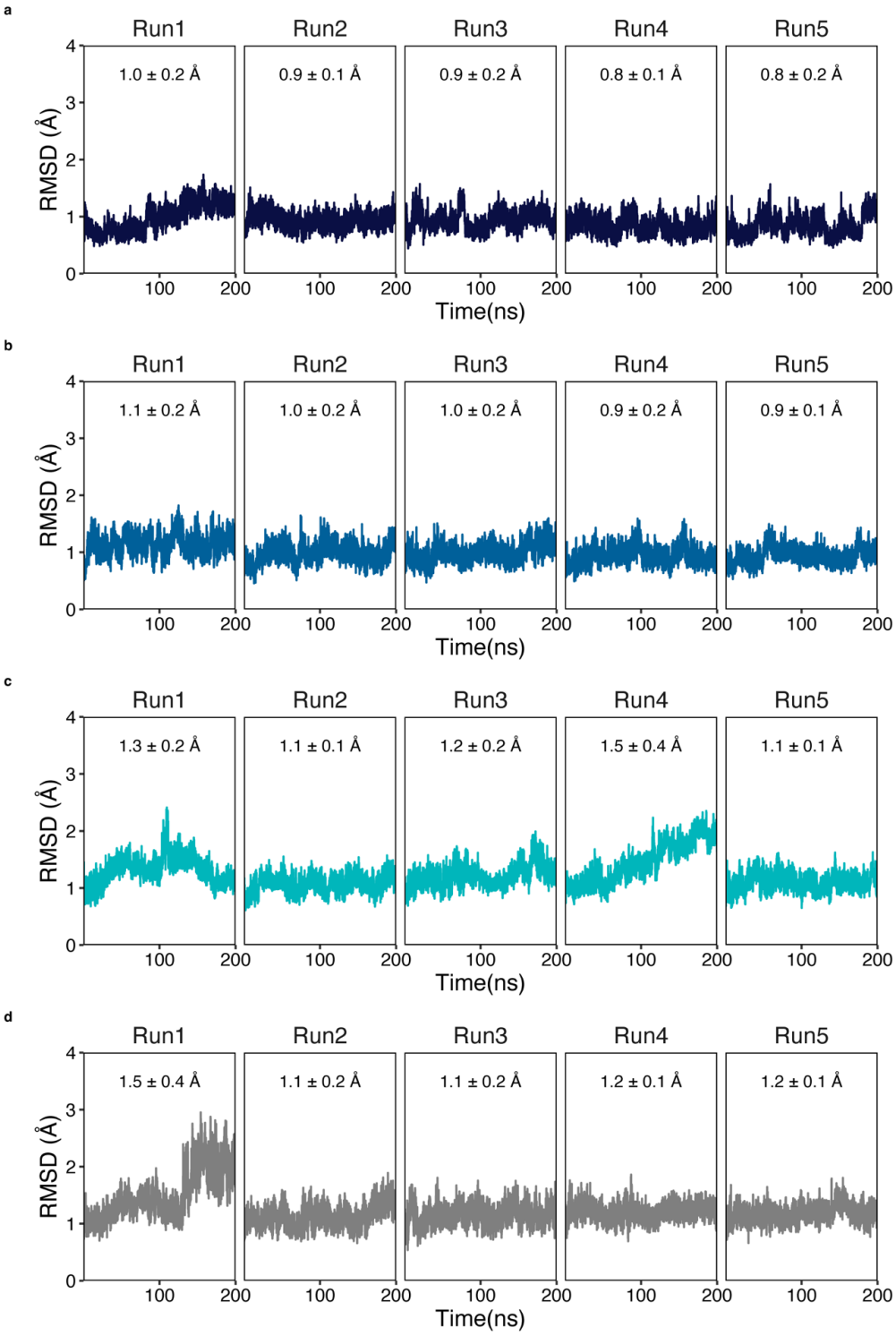

Fig. S30. RMSD values of C_α of (a) **2** and MDM2, (b) **4** and MDM2, (c) **5** and MDM2, and (d) MDM2 compared to the crystal structure during MD simulations. The results show that the MD simulations have reached well-equilibrated states and valid for further analysis.

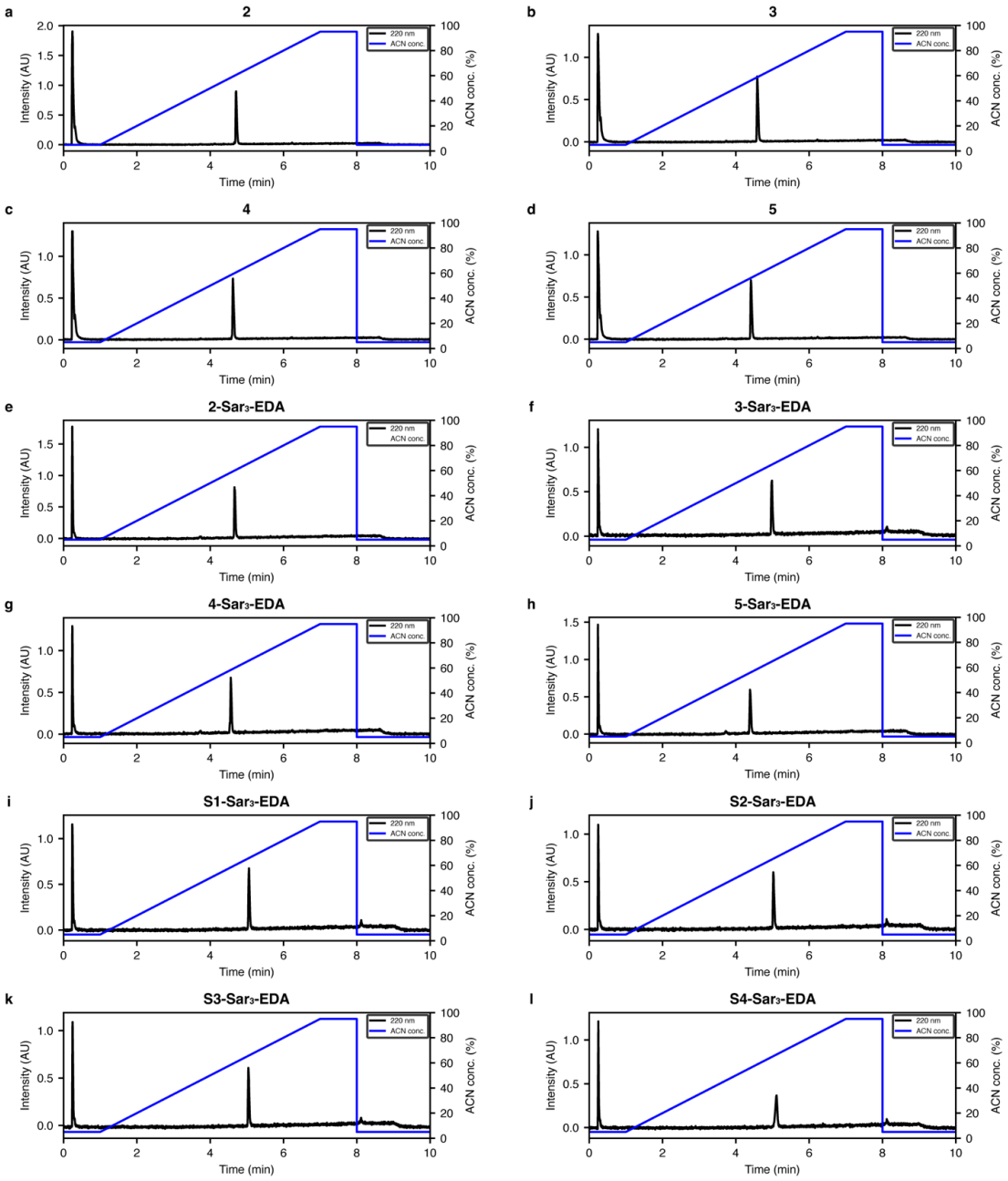

Fig. S31. UV (220 nm) chromatograms of (a–d) **2**–**5**, (e–h) **2**–**5-Sar$_3$-EDA**, **and** (i–l) **S1**–**S4-Sar$_3$-EDA** after purification measured on UPLC. The blue line denotes the percentage of ACN. The peak that appeared at 0–1 min is derived from DMSO.

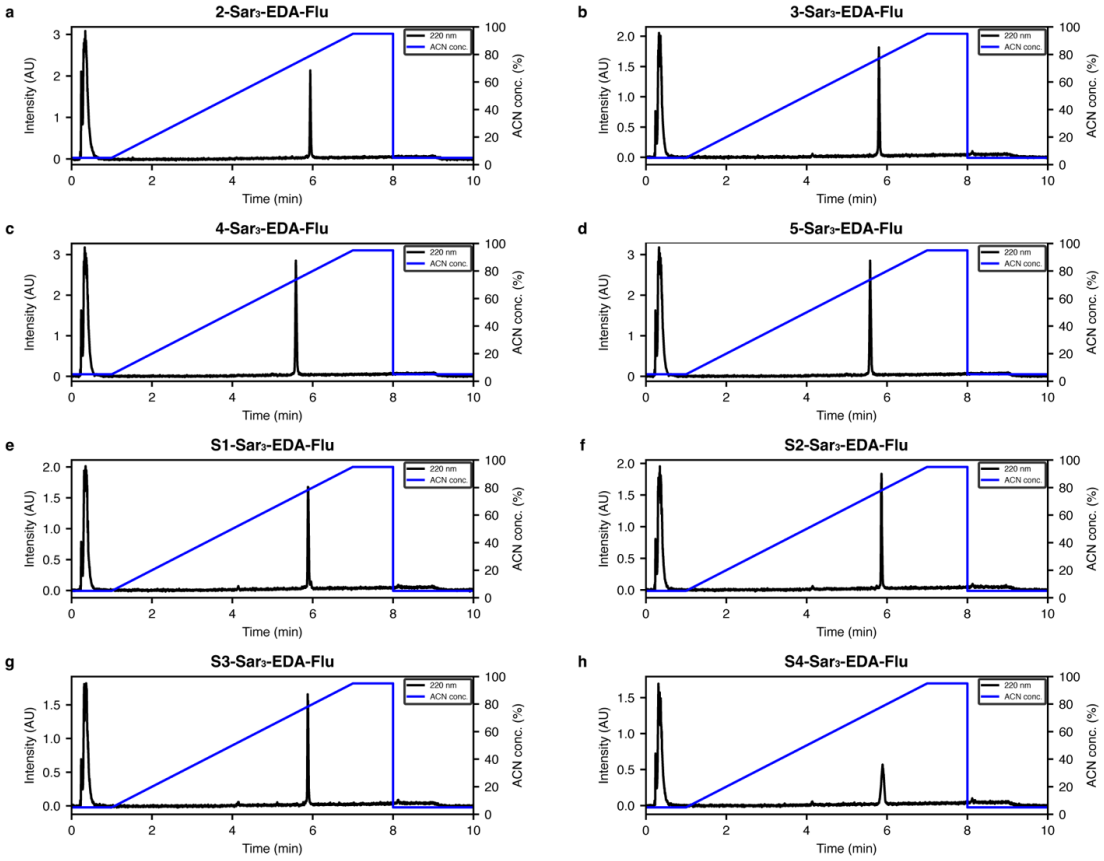

Fig. S32. UV (220 nm) chromatograms of (a–d) **2–5-Sar$_3$-EDA-Flu** and (e–h) **S1**–**S4-Sar$_3$-EDA-Flu** after purification measured on UPLC. The blue line denotes the percentage of ACN. The peak that appeared at 0–1 min is derived from DMSO.

Table S1. Crystallographic data collection and refinement statistics.

Diffraction data	
Wavelength (Å)	1.0
Resolution range (Å)	33.60 - 1.35 (1.40 - 1.35)
Space group	$P\ 2_1\ 2_1\ 2_1$
Unit cell (*a*, *b*, *c* (Å))	39.5, 45.8, 63.8
Total reflections	314,038 (17,233)
Unique reflections	26,064 (2,510)
Multiplicity	12.0 (6.9)
Completeness (%)	99.84 (98.62)
Mean $I/\sigma(I)$	20.99 (2.29)
Wilson B-factor (Å^2)	17.70
R_{merge}	0.06177 (0.821)
R_{meas}	0.06449 (0.889)
R_{pim}	0.01822 (0.3347)
$CC_{1/2}$	0.999 (0.798)
CC^*	1.000 (0.942)
Refinement statistics	
Reflections used in refinement	26,058 (2,510)
Reflections used for R_{free}	1,797 (173)
R_{work}	0.1692 (0.3116)
R_{free}	0.1897 (0.3012)
$CC_{(work)}$	0.965 (0.864)
$CC_{(free)}$	0.948 (0.871)
Number of non-hydrogen atoms	945
macromolecules	797
ligands	64
solvent	84
Protein residues	87
RMS (bonds (Å))	0.005
RMS (angles (°))	0.78
Ramachandran favored (%)	98.82
Ramachandran allowed (%)	1.18
Ramachandran outliers (%)	0.00
Rotamer outliers (%)	0.00
Clashscore	2.94
Average B-factor (Å^2)	19.95
macromolecules (Å^2)	18.64
ligands (Å^2)	20.94
solvent (Å^2)	31.63

Statistics for the highest-resolution shell are shown in parentheses.

Table S2. Chemical structures and K_D values of 2–5-Sar$_3$-EDA-Flu and S1–S4-Sar$_3$-EDA-Flu.

Compound	Chemical structure	K_D (nM)[a]
2-Sar$_3$-EDA-Flu	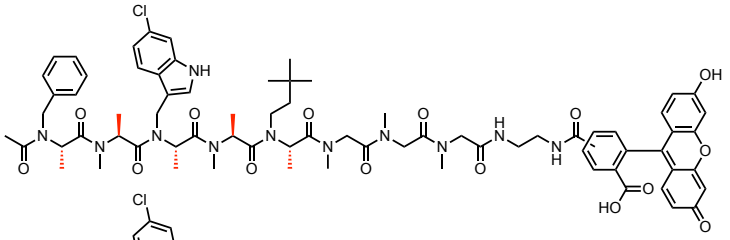	8.6
3-Sar$_3$-EDA-Flu	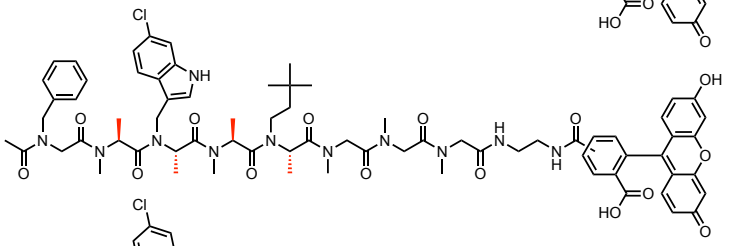	140
4-Sar$_3$-EDA-Flu	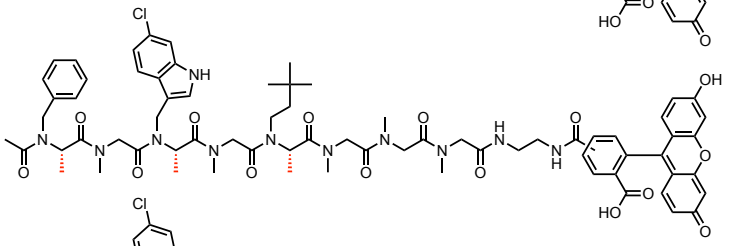	750
5-Sar$_3$-EDA-Flu	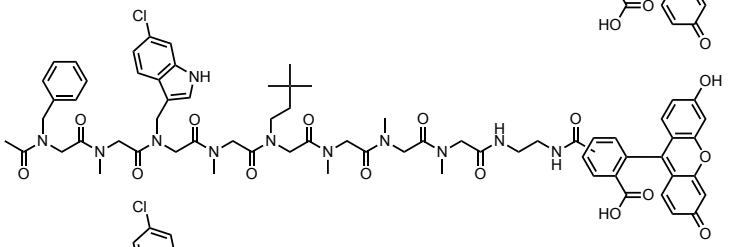	21000
S1-Sar$_3$-EDA-Flu	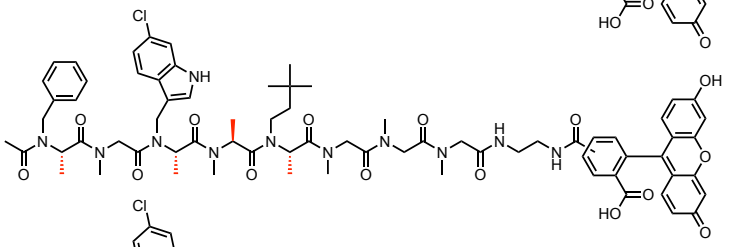	56
S2-Sar$_3$-EDA-Flu	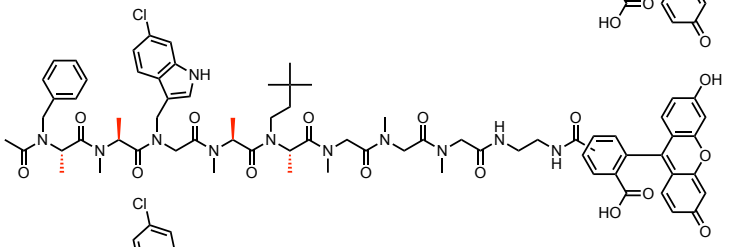	920
S3-Sar$_3$-EDA-Flu	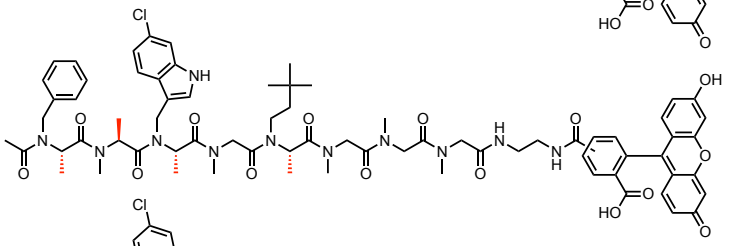	79
S4-Sar$_3$-EDA-Flu	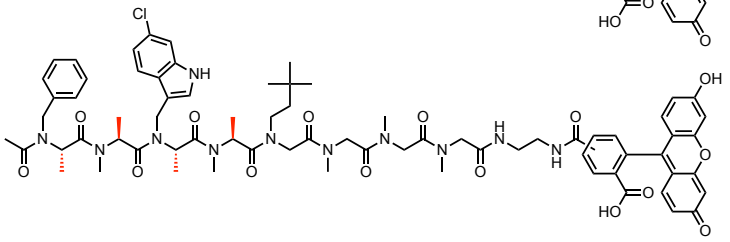	19

[a]K_D values were determined by a fluorescence anisotropy binding assay. The binding stoichiometry was assumed to be 1:1 for the fitting of the binding curve. The K_D values of **2**, **S1**, **S3**, **S4-Sar$_3$-EDA-Flu** may be subject to some error since the concentration of fluorescent peptoid probe (10 nM) is close to the K_D value.

Table S3. Chemical shifts of oligo-NSA 2 in 20% DMSO-d_6/D_2O.

Residue number	Atom	Chemical shifts (ppm)		Residue number	Atom	Chemical shifts (ppm)	
		ttt[a]	ctt[a]			ttt[a]	ctt[a]
0	HA	2.14	2.27	3	CR2	139.5	139.5
0	CA	24.1	23.5	3	CR3	122.3	122.3
0	C	177.1	177.1	3	CS2	114.5	114.5
1	HA	4.96	4.63	3	CS3	122.9	122.9
1	HB	0.78	0.98	3	CT2	126.9	126.9
1	HO1	4.54	4.13	3	C	175.8	175.8
1	HO2	4.54	4.62	4	HA	4.67	4.67
1	HQ	7.17	7.06	4	HB	1.10	1.10
1	HR	7.29	7.29	4	HO	3.00	3.00
1	HS	7.23	7.23	4	CA	53.6	53.6
1	CA	53	57.1	4	CB	16.7	16.7
1	CB	16.3	17.3	4	CO	33.4	33.4
1	CO	50.9	48.2	4	C	176.4	176.4
1	CP	139.7	139.7	5	HA	5.23	5.23
1	CQ	129	129.8	5	HB	1.25	1.25
1	CR	131.7	131.7	5	HO1	3.16	3.16
1	CS	130.4	130.4	5	HO2	3.36	3.36
1	C	174.6	174.6	5	HP1	1.4	1.4
2	HA	5.03	4.73	5	HP2	1.4	1.4
2	HB	0.99	0.74	5	HR	0.81	0.81
2	HO	2.85	2.81	5	CA	52.9	52.9
2	CA	53.5	51.2	5	CB	17	17
2	CB	16.6	16.6	5	CO	43.4	43.4
2	CO	33	32.8	5	CP	45.7	45.7
2	C	176.3	176.3	5	CR	31.3	31.3
3	HA	5.33	5.33	5	C	173.9	173.9
3	HB	1.31	1.31	6	HX11	3.48	3.48
3	HO1	4.74	4.74	6	HX12	3.48	3.48
3	HO2	4.74	4.74	6	HX21	3.53	3.53
3	HQ1	7.18	7.18	6	HX22	3.66	3.66
3	HR3	7.52	7.52	6	HY11	2.94	2.94
3	HS2	7.54	7.54	6	HY12	2.94	2.94
3	HS3	7.18	7.18	6	HY21	2.94	2.94
3	CA	54.1	54.1	6	HY22	2.94	2.94
3	CB	16.3	16.3	6	CX1	47.3	47.3
3	CO	43.1	43.1	6	CX2	44.2	44.2
3	CP	114.6	114.6	6	CY1	46.6	46.6
3	CQ1	125.8	125.8	6	CY2	46.6	46.6
3	CQ2	130.2	130.2				

[a]The definitions of these states are shown in Fig. S2.

Table S4. Chemical shifts of oligo-NSA/G 3 in DMSO-*d*$_6$.

Residue number	Atom	Chemical shift (ppm)					
		ttt[a]	ctt[a]	tct[a]	cct[a]	ttc[a]	ctc[a]
0	HA	2.03	1.88	2.08	1.96	2.03	1.90
0	C	173.6	174.2	173.6	174.2	173.6	174.2
0	CA	24.3	24.3	24.3	24.4	24.3	25.0
1	HA1	4.02	4.19	4.14	4.27	4.06	4.21
1	HA2	4.13	4.19	4.02	4.27	4.14	4.21
1	HO1	4.39	4.33	4.56	4.39	4.39	4.33
1	HO2	4.53	4.37	4.64	4.50	4.53	4.37
1	HQ	7.25	7.25	7.25	6.89	7.25	7.25
1	HR	7.41	7.34	7.41	7.28	7.41	7.34
1	HS	7.34	7.28	7.34	7.28	7.34	7.28
1	C	170.9	171.1	171.5	171.9	171	171.2
1	CA	50.4	52.8	50.4	53.0	50.5	52.8
1	CO	55.4	52.6	55.4	52.5	55.4	52.6
1	CP	140.6	141	140.5	141	140.6	140.6
1	CQ#	129.9	130.8	129.9	130.2	129.9	130.8
1	CR#	131.8	131.4	131.8	130.8	131.8	131.4
1	CS	130.4	130.1	130.4	130.1	130.4	130.1
2	HA	5.51	5.52	5.6	5.58	5.51	5.55
2	HB	1.23	1.23	1.29	1.34	1.23	1.23
2	HO	2.88	2.88	2.94	2.99	2.89	2.90
2	C	173.8	173.8	174.0	174.4	173.7	173.8
2	CA	52.1	51.8	51.0	51.4	51.7	52.0
2	CB	18.0	18.0	18.5	18.7	18.0	18.0
2	CO	32.2	32.2	32.2	32.3	32.4	32.4
3	HA	5.31	5.31	4.98	5.01	4.97	4.99
3	HB	1.16	1.16	1.29	1.31	1.16	1.16
3	HO1	4.62	4.62	4.48	4.51	4.65	4.65
3	HO2	4.74	4.74	4.61	4.56	4.77	4.77
3	HQ1	7.25	7.25	7.19	7.13	7.32	7.32
3	HR3	7.49	7.49	7.5	7.55	7.49	7.49
3	HS2	7.44	7.44	7.41	7.41	7.44	7.44
3	HS3	7.05	7.05	6.99	6.99	7.05	7.05
3	C	173.0	173.0	172	171.9	172.9	172.9
3	CA	52.9	52.9	53.7	56.1	53.7	56.0
3	CB	18.4	18.4	20.7	20.7	18.4	18.4
3	CO	42.0	42.0	40.8	40.5	42.6	42.6
3	CP	115.1	115.1	115.3	115.1	115.3	115.3
3	CQ1	126.7	126.7	128.5	128.6	127.5	127.5
3	CQ2	127.6	127.6	127.7	127.7	127.6	127.6
3	CR3	122.7	122.7	123.1	123.1	122.7	122.7

Residue number	Atom	Chemical shift (ppm)					
		ttt[a]	ctt[a]	tct[a]	cct[a]	ttc[a]	ctc[a]
3	CS2	114.3	114.3	114.3	114.3	114.3	114.3
3	CS3	122.1	122.1	121.9	121.9	122.1	122.1
4	HA	4.80	4.80	4.90	4.87	5.14	5.10
4	HB	0.72	0.72	0.68	0.59	0.76	0.73
4	HO	2.85	2.85	2.66	2.69	2.74	2.72
4	C	173.6	173.6	173.9	174.3	173.4	173.4
4	CA	51.9	51.9	52.3	52	51.2	51.2
4	CB	17.4	17.4	17.5	17.4	17.5	17.5
4	CO	33	33	32.6	32.7	32.7	32.7
5	HA	5.27	5.27	5.27	5.27	4.73	4.73
5	HB	1.10	1.10	1.10	1.10	1.26	1.26
5	HO1	3.00	3.00	3.11	3.10	3.08	3.08
5	HO2	3.29	3.29	3.46	3.53	3.23	3.23
5	HP1	1.29	1.29	1.41	1.41	1.33	1.33
5	HP2	1.29	1.29	1.41	1.41	1.33	1.33
5	HR	0.81	0.81	0.95	0.95	0.87	0.87
5	C	171.4	171.4	171.4	171.4	170.8	170.8
5	CA	50.9	50.9	50.9	50.9	55.2	55.2
5	CB	18.4	18.4	18.4	18.4	20.9	20.9
5	CO	42.1	42.1	42.4	42.4	43.5	43.5
5	CP	46.1	46.1	46.3	46.3	44.6	44.6
5	CQ	32.6	32.6	32.8	32.8	32.8	32.8
5	CR	32.1	32.1	32.2	32.2	32.2	32.2
6	HX11	3.15	3.15	3.15	3.15	3.08	3.08
6	HX12	3.21	3.21	3.21	3.21	3.29	3.29
6	HX21	3.32	3.32	3.32	3.32	3.09	3.09
6	HX22	3.43	3.43	3.43	3.43	3.58	3.58
6	HY11	2.60	2.60	2.60	2.60	2.55	2.55
6	HY12	2.64	2.64	2.64	2.64	2.55	2.55
6	HY21	2.66	2.66	2.66	2.66	2.69	2.69
6	HY22	2.66	2.66	2.66	2.66	2.69	2.69
6	CX1	48.8	48.8	48.8	48.8	49.0	49.0
6	CX2	45.7	45.7	45.7	45.7	45.9	45.9
6	CY1	48.6	48.6	48.6	48.6	48.7	48.7
6	CY2	48.2	48.2	48.2	48.2	48.4	48.4

[a]The definitions of these states are shown in Fig. S6.

Table S5. Chemical shifts of oligo-NSA/G 4 in 20% DMSO-d_6/D_2O.

Residue number	Atom	Chemical shifts (ppm)	
		ttt[a]	ctt[a]
0	HA	2.23	2.35
0	C	176.9	177
0	CA	24.2	23.6
1	HA	5.55	5.06
1	HB	1.24	1.37
1	HO1	4.44	-
1	HO2	4.73	-
1	HQ	7.11	7.11
1	HR	7.14	7.14
1	C	175	175
1	CA	51.5	56.1
1	CB	16.4	17.4
1	CO	50.7	50.7
1	CQ	129.1	129.1
1	CR	131.4	131.4
2	HA1	3.49	3.28
2	HA2	3.7	3.32
2	HO	2.94	2.89
2	C	173	173
2	CA	53.1	53.3
2	CO	39.3	39.2
3	HA	5.5	5.5
3	HB	1.3	1.3
3	HO1	4.63	4.63
3	HO2	4.63	4.63
3	HQ1	7.23	7.23
3	HR3	7.6	7.6
3	HS2	7.62	7.62
3	HS3	7.24	7.24
3	C	175.6	175.6
3	CA	52.8	52.8
3	CB	16.9	16.9
3	CO	42.6	42.6
3	CP	113.9	113.9
3	CQ1	126.4	126.4
3	CR3	122.3	122.3
3	CS2	114.5	114.5
3	CS3	122.7	122.7
4	HA1	3.9	3.9
4	HA2	4.13	4.13
4	HO	3.07	3.07
4	C	172.1	172.1
4	CA	53.1	53.1
4	CO	39.6	39.6
5	HA	5.29	5.29
5	HB	1.29	1.29
5	HO1	3.24	3.24
5	HO2	3.24	3.24
5	HP1	1.35	1.35
5	HP2	1.51	1.51
5	HR	0.88	0.88
5	C	174	174
5	CA	52.8	52.8
5	CB	17	17
5	CO	43.3	43.3
5	CP	45.6	45.6
5	CR	31.2	31.2
6	HX11	3.52	3.52
6	HX12	3.52	3.52
6	HX21	3.63	3.63
6	HX22	3.63	3.63
6	HY11	2.96	2.96
6	HY12	2.96	2.96
6	HY21	2.96	2.96
6	HY22	2.96	2.96
6	CX1	47.1	47.1
6	CX2	43.9	43.9
6	CY1	46.4	46.4
6	CY2	46.4	46.4

[a]The definitions of these states are shown in Fig. S11.

Table S6. Chemical shifts of oligo-NSG 5 in 20% DMSO-d_6/D_2O.

Residue number	Atom	Chemical shifts (ppm)
0	HA	2.21
0	C	177.5
0	CA	23.4
1	HA1	4.24
1	HA2	4.30
1	HO1	4.58
1	HO2	4.58
1	HQ	7.27
1	HR	7.39
1	HS	7.32
1	C	172.6
1	CA	50.2
1	CO	55.9
1	CP	138.7
1	CQ	129.7
1	CR	131.6
1	CS	130.5
2	HA	4.51
2	HO	3.00
2	C	173.0
2	CA	53.0
2	CO	38.4
3	HA1	4.16
3	HA2	4.38
3	HO1	4.72
3	HO2	4.72
3	HQ1	7.11
3	HR3	7.37
3	HS2	7.54
3	HS3	7.10
3	C	173.6
3	CA	52.2
3	CO	46.4
3	CP	112.0
3	CQ1	128.0
3	CR3	122.6
3	CS2	114.4
3	CS3	122.8
4	HA1	4.13
4	HA2	4.25
4	HO	2.94
4	C	172.1
4	CA	52.3
4	CO	38.6
5	HA1	4.22
5	HA2	4.22
5	HO1	3.26
5	HO2	3.26
5	HP1	1.51
5	HP2	1.51
5	HR	0.92
5	C	170.8
5	CA	50.6
5	CO	48.3
5	CP	43.5
5	CR	31.2
6	HX11	3.52
6	HX12	3.52
6	HX21	3.59
6	HX22	3.59
6	HY11	2.93
6	HY12	2.93
6	HY21	2.93
6	HY22	2.93
6	CX1	47.1
6	CX2	44.3
6	CY1	46.7
6	CY2	46.7

References

1. M. J. Frisch, G. W. Trucks, H. B. Schlegel, G. E. Scuseria, M. a. Robb, J. R. Cheeseman, G. Scalmani, V. Barone, G. a. Petersson, H. Nakatsuji, X. Li, M. Caricato, a. V. Marenich, J. Bloino, B. G. Janesko, R. Gomperts, B. Mennucci, H. P. Hratchian, J. V. Ortiz, a. F. Izmaylov, J. L. Sonnenberg, Williams, F. Ding, F. Lipparini, F. Egidi, J. Goings, B. Peng, A. Petrone, T. Henderson, D. Ranasinghe, V. G. Zakrzewski, J. Gao, N. Rega, G. Zheng, W. Liang, M. Hada, M. Ehara, K. Toyota, R. Fukuda, J. Hasegawa, M. Ishida, T. Nakajima, Y. Honda, O. Kitao, H. Nakai, T. Vreven, K. Throssell, J. a. Montgomery Jr., J. E. Peralta, F. Ogliaro, M. J. Bearpark, J. J. Heyd, E. N. Brothers, K. N. Kudin, V. N. Staroverov, T. a. Keith, R. Kobayashi, J. Normand, K. Raghavachari, a. P. Rendell, J. C. Burant, S. S. Iyengar, J. Tomasi, M. Cossi, J. M. Millam, M. Klene, C. Adamo, R. Cammi, J. W. Ochterski, R. L. Martin, K. Morokuma, O. Farkas, J. B. Foresman and D. J. Fox, 2016, Gaussian, Inc., Wallin.
2. T. D. Goddard, C. C. Huang, E. C. Meng, E. F. Pettersen, G. S. Couch, J. H. Morris and T. E. Ferrin, *Protein Sci.*, 2018, **27**, 14–25.
3. E. F. Pettersen, T. D. Goddard, C. C. Huang, E. C. Meng, G. S. Couch, T. I. Croll, J. H. Morris and T. E. Ferrin, *Protein Sci.*, 2021, **30**, 70–82.
4. E. C. Meng, T. D. Goddard, E. F. Pettersen, G. S. Couch, Z. J. Pearson, J. H. Morris and T. E. Ferrin, *Protein Sci.*, 2023, **32**.
5. E. F. Pettersen, T. D. Goddard, C. C. Huang, G. S. Couch, D. M. Greenblatt, E. C. Meng and T. E. Ferrin, *J Comput Chem*, 2004, **25**, 1605–1612.
6. J. Morimoto, Y. Fukuda, D. Kuroda, T. Watanabe, F. Yoshida, M. Asada, T. Nakamura, A. Senoo, S. Nagatoishi, K. Tsumoto and S. Sando, *J. Am. Chem. Soc.*, 2019, **141**, 14612–14623.
7. Y. Fukuda, M. Yokomine, D. Kuroda, K. Tsumoto, J. Morimoto and S. Sando, *Chem Sci*, 2021, **12**, 13292–13300.
8. M. Yokomine, J. Morimoto, Y. Fukuda, Y. Shiratori, D. Kuroda, T. Ueda, K. Takeuchi, K. Tsumoto and S. Sando, *Angew. Chem.-Int. Edit.*, 2022, **61**, e202200119.
9. K. Hirata, K. Yamashita, G. Ueno, Y. Kawano, K. Hasegawa, T. Kumasaka and M. Yamamoto, *Acta Crystallogr. Sect. D-Struct. Biol*, 2019, **75**, 138–150.
10. W. Kabsch, *Acta Crystallogr. Sect. D-Biol. Crystallogr.*, 2010, **66**, 125–132.
11. K. Yamashita, K. Hirata and M. Yamamoto, *Acta Crystallogr. Sect. D-Struct. Biol*, 2018, **74**, 441–449.
12. Y. H. Lau, Y. Wu, M. Rossmann, B. X. Tan, P. de Andrade, Y. S. Tan, C. Verma, G. J. McKenzie, A. R. Venkitaraman, M. Hyvönen and D. R. Spring, *Angew. Chem.-Int. Edit.*, 2015, **54**, 15410–15413.
13. D. Liebschner, P. V. Afonine, M. L. Baker, G. Bunkoczi, V. B. Chen, T. I. Croll, B. Hintze, L. W. Hung, S. Jain, A. J. McCoy, N. W. Moriarty, R. D. Oeffner, B. K. Poon, M. G. Prisant, R. J. Read, J. S. Richardson, D. C. Richardson, M. D. Sammito, O. V. Sobolev, D. H. Stockwell, T. C. Terwilliger, A. G. Urzhumtsev, L. L. Videau, C. J. Williams and P. D. Adams, *Acta Crystallogr. Sect. D-Struct. Biol*, 2019, **75**, 861–877.
14. 14 M. D. Winn, C. C. Ballard, K. D. Cowtan, E. J. Dodson, P. Emsley, P. R. Evans, R. M. Keegan, E. B. Krissinel, A. G. W. Leslie, A. McCoy, S. J. McNicholas, G. N. Murshudov, N. S. Pannu, E. A. Potterton, H. R. Powell, R. J. Read, A. Vagin and K. S. Wilson, *Acta Crystallogr. Sect. D-Biol. Crystallogr.*, 2011, 67, 235–242.
15. W. Borcherds, F. Theillet, A. Katzer, A. Finzel, K. M. Mishall, A. T. Powell, H. Wu, W. Manieri, C. Dieterich, P. Selenko, A. Loewer and G. W. Daughdrill, *Nat. Chem. Biol.*, 2014, **10**, 1000–1002.
16. D. A. Case, H. M. Aktulga, K. Belfon, I. Y. Ben-Shalom, J. T. Berryman, S. R. Brozell, D. S. Cerutti, I. T. E. Cheatham, G. A. Cisneros, V. W. D. Cruzeiro, T. A. Darden, R. E. Duke, G. Giambasu, M. K. Gilson, H. Gohlke, A. W. Goetz, R. Harris, S. Izadi, S. A. Izmailov, K. Kasavajhala, M. C. Kaymak, E. King, A. Ko-Valenko, T. Kurtzman, T. S. Lee, S. LeGrand, P. Li, C. Lin, J. Liu, T. Luchko, R. Luo, M. Machado, V. Man, M. Manathunga, K. M. Merz, Y. Miao, O. Mikhailovskii, G. Monard, H. Nguyen, K. A. O'Hearn, A. Onufriev, F. Pan, S. Pantano, R. Qi, A. Rahnamoun, D. R. Roe, A. Roitberg, C. Sagui, S. Schott-Verdugo, A. Shajan, J. Shen, C. L. Simmerling, N. R. Skrynnikov, J. Smith, J. Swails, R. C. Walker, J. Wang, J. Wang, H. Wei, R. M. Wolf, X. Wu, Y. Xiong, Y. Xue, D. M. York, S. Zhao and P. A. Kollman, 2022.
17. T. Darden, D. York and L. Pedersen, *J. Chem. Phys.*, 1993, **98**, 10089–10092.
18. B. Webb and A. Sali, *Curr. Protoc. Bioinf.*, 2016, **54**, 5.6.1-5.6.37.